Journal of Renewable Energy and Sustainable Development (RESD) Volume 12, Issue 1, June 2026 - ISSN 2356-8569
http://dx.doi.org/10.21622/RESD.2026.12.1.1889

Received: 06 January 2026 Accepted: 08 May 2026 Published: 07 June 2026

Design and Real-Time Implementation of an ANN-Driven MPPT Controller for Hybrid Renewable Energy Systems

Mohamed El-Sayed M. Essa [1*], Hemdan S. El-sayed [2], Elwy E. El-kholy [3], Hilmy El- sayed Awad [4], and Mohamed Saleh Elsayed [5]

[1*] Ministry of Civil Aviation, Egyptian Aviation Academy, Institute of Aviation Engineering and Technology, Electrical Power and Machines Dept., Imbaba Airport, Giza, Egypt

[2,4] Helwan University, Faculty of Technology and Education, Department of Electrical Engineering, Cairo, Egypt

[3] Menoufia University, Faculty of Engineering, Electrical Engineering, Al-Menoufiya, Egypt

[5] Zagazig University, Faculty of Engineering, Aeronautical Engineering Department, Zagazig, Al-Sharqia, Egypt

mohamed.essa@iaet.edu.eg, hamzahemdan74@gmail.com, eelkholy63@yahoo.com, hilmy_awad@yahoo.com, m_saleh_99@yahoo.com

Abstract

Enhancing the reliability and efficiency of hybrid renewable systems (HES) under dynamic environmental conditions requires efficient and effective control for power extraction. Conventional methods of maximum power point tracking (MPPT) often suffer from limited accuracy and slow response when dealing with rapid variations in temperature and irradiance and nonlinear characteristics. For this issue, this paper proposes a distinct and improved MPPT approach based on the artificial neural network (ANN) technique. The suggested MPPT – based ANN is trained and built based on collected data used from the traditional IC technique. The proposed approaches are implemented on a grid-connected 150-kW hybrid PV/wind energy system. The objective of the control is to ensure optimal power extraction despite temperature, solar irradiation, and wind speed variations. In addition, fractional order proportional-integral-derivative (FOPID) controllers are designed for inverter control to enhance voltage regulation and, hence, power quality. Additionally, the performance of incremental conductance (IC) and ANN techniques is compared using detailed MATLAB/Simulink simulations. The experimental real-time validation is performed through an investigation based on the OPAL-RT 4512 hardware-in-the-loop platform. The results demonstrate that the MPPT – based ANN significantly outperforms in terms of tracking speed, dynamic stability, and steady-state accuracy in a simulation study and experiment validation. Hence, the originality of this work is to integrate the MPPT – based ANN technique for a hybrid PV/wind framework and inverter control based on FOPID through simulation and real-time hardware-in-the-loop (HIL) validation, which offers a robust and high-efficiency solution for rapidly time-varying environmental conditions.

Index-words: *PV System, Wind System, MPPT, ANN, Hardware-in-the-loop, OPAL-RT 4512, FOPID.*

I. Introduction

Renewable energy sources, particularly solar and wind, are increasingly vital due to their ability to reduce greenhouse gas emissions, improve air quality, and promote energy security. Both solar and wind power had a significant economic impact and decreased health risks by reducing pollutants like sulfur dioxide and nitrogen oxides [1]. New and renewable energy sources not only reduce reliance on fossil fuels but also add diversity to the electrical power mix. Thus, such technology also enhances energy security because it reduces reliance on finite resources, which are very susceptible to geopolitical instability [2]. Likewise, new and renewable energy technologies will be able to contribute to frugal growth and jobs, as well as citizens' health by reducing air pollution and environmental degradation. Along with increasing global demand for energy, there is an urgent need to make our energy future more sustainable, emphasizing developing and deploying new and renewable sources of energy in our endeavors [3].

* Corresponding author

http://dx.doi.org/10.21622/RESD.2026.12.1.1889

Hybrid Energy Systems (HES) integrate traditional and renewable sources and are often grid-connected to reduce reliance on storage. Their key advantages include lowering costs, meeting AC load demands, and alleviating grid congestion. To ensure efficiency, specialized controllers maximize power output based on variations in load and climate while maintaining synchronization with the grid [4]. As a technical solution, using trackers to connect the hybrid system to the common AC bus is recommended. The AC bus will be used to connect these two energy sources to the electrical grid, as illustrated in Fig. 1. To ensure a balanced output power, the hybrid system utilizes wind turbines to supplement the power when the weather conditions are either very windy or at low light intensities, while photovoltaic panels generate electrical energy in sunny conditions [5]. The system maximizes renewable energy integration to utilize traditional grid electricity while reducing dependence on it, particularly when demand is high. Additionally, the hybrid architecture reduces the stress for the grid and allows for further improvement of the overall efficiency of the system by using weather-dependent energy contributions [6]. It is well known that with the development of modern innovative technologies, renewable energy sources will occupy a pivotal position in solving many energy problems and energy systems around the world [7]. As a result, many scientific studies have been published in this field, which present many methods of tracking the maximum power point (MPPT) to maximize the energy generated from these renewable sources. Some of these methods are traditional, while others are modern, such as artificial intelligence (AI) -based technologies like ANNs. There is still a lack of published studies on the dynamic performance of MPPT systems in grid-connected hybrid PV/wind systems under varying environmental conditions, despite the existence of numerous research studies addressing MPPT methods in single-source or standalone systems [8]. Consequently, most recent studies have overlooked important impacts on grid power quality, such as stability and voltage distortion, focusing solely on power output or MPPT efficiency. Additionally, hybrid MPPT strategies have not been evaluated under real-time variations in wind power and solar irradiation. In complex nonlinear environments, new intelligent techniques have proven to perform better [9]. In addition, there is a lack of a thorough framework for evaluating MPPT performance in grid-connected hybrid PV/wind systems under dynamically shifting circumstances, where designing and implementing reliable grid-integrated renewable energy systems is ultimately hampered by this gap [10].

There is no constant evaluation framework for hybrid PV/wind systems that takes grid-side performance and energy conversion efficiency into account. The system optimization is still lacking if the effects of these techniques on grid current quality, voltage stability, and dynamic response under changing environmental conditions are not properly analyzed; because of this, creating hybrid systems that are reliable, grid-compliant, and efficient is difficult. This paper, therefore, aims to evaluate and compare the performance of two MPPT control techniques within a grid-connected hybrid PV/wind system. Furthermore, its objective is to analyze their effectiveness in not only maximizing power output but also improving grid power quality, minimizing total harmonic distortion, and ensuring fast dynamic response under varying environmental conditions. Also, the results aim at identifying the most efficient and grid-friendly MPPT strategy for future renewable integrations.

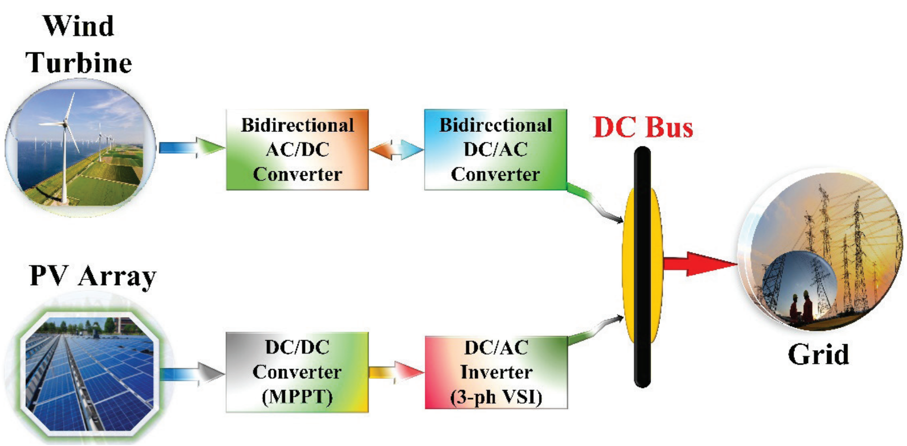

Figure 1: Proposed configuration of grid-connected HES.

II. Literature review

Using an abundance of solar and wind resources, the proposed study aims to develop, manage, and obtain access to a PV/wind crossbred system connected to the grid-tied for the Gabel El-Zeit area of Egypt, which is studied in [11]. It is the system that can boost reliability, reduce costs, and improve sustainability by producing a control approach to maximize output power and stability of the grid. Furthermore, the findings are studied in [12], which also deals with a model for including renewable energy in similar regions. An investigation of a hybrid system of renewable energy that integrates battery storage systems, wind turbines, and PV cells is discussed in [13]. Furthermore, [14] presents a designed standalone system with a PV/wind microgrid power system to generate dependable off-grid power. A grid-connected PV/wind power system in Dongola, Sudan, is proposed with performance evaluation and control design as demonstrated in [15]. In addition, a hybrid PV/wind system connected to the grid-tied for the Adrar region of Algeria is also discussed in [16].

In [17], AI is proposed to manage the hybrid renewable energy sources in microgrids efficiently. So, AI improves energy management, load forecasting, and fault detection, helping to create more resilient and intelligent microgrids. A hybrid system that combines doubly-fed induction generator (DFIG)-based wind turbine batteries, PV panels, and an alternating current (AC) and direct current (DC) grid connection is established in [18] to develop the performance of the system. Another example is a small hybrid grid-connected system, combining PV solar power, wind power, and batteries, and using MPPT technology based on an ANN trained using the Levenberg-Marquardt algorithm. Through inductor-capacitor-inductor (LCL) filters, this grid guarantees high power quality, a stable DC bus voltage, and optimal energy extraction [19]. In a similar manner, authors in [20] use an intelligent fractional-order controller that governs superconducting magnetic energy storage (SMES) systems in microgrids that utilize sources of renewable energy.

A centralized DC architecture with strong grid integration based on an ANN approach for MPPT for the system of hybrid PV-wind-battery is described in [21]. Besides, authors in [22] compare different training algorithms for ANN, such as Levenberg–Marquardt (LM), scaled conjugate gradient (SCG), and Bayesian regularization (BR) techniques, to examine ANN-based MPPT for solar EV charging. Thus, the findings demonstrate that SCG provides better tracking speed, less oscillation, and increased efficiency for wireless charging infrastructure. To improve PV efficiency and power quality, the study in [23] suggests a dual ANN-based MPPT and power conditioning framework that achieves ultra-low THD (less than 1.73%) and strong stability. Moreover, a particle swarm optimization (PSO) based ANN controller is proposed for sensorless MPPT in hybrid PV/wind systems as in [24]. By employing DC-link behavior, it maximizes efficiency and reduces THD (2–3%), guaranteeing stability in both grid-connected and islanded modes. Table 1 demonstrates a systematic review of recent studies on HES. Despite the extensive research on MPPT approaches that have been proposed for HES, traditional techniques such as IC still suffer from slow convergence, lower accuracy, and oscillations for the steady-state duration under fast variation in the environment. Intelligent methods, comprising ANN and fuzzy logic, partially address these issues in the case of limited data or simple variation in irradiation and temperature. Furthermore, many existing papers are limited to simulation studies without appropriate experimental validation, decreasing their real-world applicability. Besides, there is a lack of hybrid strategies that efficiently integrate adaptive methods like ANN with traditional techniques to achieve both high efficiency and fast response. This gap is mainly significant in HES, where most existing research lacks real-time HIL validation using OPAL- RT 4512 systems, decreasing confidence in their real-world implementation.

This paper proposes an enhanced technique for MPPT based on the integration of IC with an ANN to improve tracking performance in HES. The proposed technique is assessed under variable irradiation and temperature conditions to guarantee robustness in environmental variations. The evaluation of performance is performed using significant metrics such as MPPT efficiency, percentage of tracking error, different error metrics, and dynamic response. The system is investigated using MATLAB\ SIMULINK package for a simulation study, while HIL experimental validation is implemented using an OPAL- RT 4512 system to approve practical applicability. Besides, the manuscript depicts a configuration of grid-connected, indicating the value of the suggested

Volume 12, Issue 1, June 2026 - ISSN 2356-8569
http://dx.doi.org/10.21622/RESD.2026.12.1.1889

technique in real-world power systems. The results demonstrate distinct enhancements in decreasing oscillations, improving speed of response, and increasing the overall efficiency compared to the IC approach.

Table 1: Comprehensive analysis for recent control of HES

Reference	Objective	Control Technique	System Configuration	Simulation Platform	Hybrid Coordination	Dynamic Conditions	Performance Metrics	Key Innovation
[17], 2023	Improve electricity reliability and sustainability in remote areas.	Artificial Intelligence (AI), ANN, PSO.	Hybrid PV-Wind systems with BESS and grid integration.	Case study simulation platform.	AI is used for system optimization and grid integration.	Variations in RESs, intermittency, and weather conditions.	System accuracy, reduced error (NMSE 1.10%).	-Use of AI and optimization techniques to enhance prediction and control, improving system performance.
[18], 2023	Reduce CO2 emissions by enhancing renewable power systems.	Neuro-Fuzzy Direct Power Control (NF-DPC), Fuzzy Controller (FC), Modified Fuzzy Direct Power Control (MF-DPC), Energy Management.	PV-Wind system with battery storage, grid-side converter, and DFIG wind turbine.	MATLAB/ Simulink.	Energy management, power control between wind, PV, and battery.	Variations in wind speed, solar irradiance, and load demand.	Reduction of THD (64%), active/ reactive power ripple reduction (72%, 50%), and THD less than 4%.	-Improved power quality, reduced THD, and enhanced equipment lifespan with energy management.
[19], 2023	To design and implement a grid-connected hybrid microgrid for reliable energy management and maximum power extraction.	ANN-based MPPT for DC Boost converters of duty cycle control.	Hybrid PV, Wind Energy Conversion System (WECS), and Battery Energy Storage (BESS).	MATLAB/ Simulink.	Coordinated control based on Battery State of Charge (SOC) and PV current output.	Varying environmental factors (irradiation/ wind) and fluctuating load conditions.	Harmonic reduction, MPPT efficiency, and DC bus voltage stability.	-Use of the Levenberg–Marquardt algorithm to optimize ANN training for more accurate and faster MPPT.
[20], 2024	Improve energy management and performance of a standalone microgrid.	Fractional-order proportional integral (FOPI) controller, intelligent FOPI (iFOPI), dandelion optimizer (DO).	SMES, wind energy devices, energy storage battery, FOPI+iFOPI control for voltage and current regulation.	MATLAB simulations.	Energy management with FOPI+iFOPI for voltage and frequency regulation.	Wind speed and load variations, step changes in load and wind speed.	Constant AC power, accurate load demand, voltage, and frequency stability.	-Use of the FOPI+iFOPI controller with SMES for improved performance and stability over the conventional PI controller.
[21], 2025	Design and simulation of a grid-connected hybrid PV-wind-battery system.	ANN-based MPPT and intelligent energy management strategy.	PV, WECS, and BESS via a centralized DC bus architecture	MATLAB/ Simulink.	Real-time coordination based on generation and battery SOC.	Variable wind speed and solar irradiation conditions.	Power flow stability, response speed, and MPPT efficiency.	-Higher efficiency and faster response using ANN compared to conventional MPPT.

Volume 12, Issue 1, June 2026 - ISSN 2356-8569
http://dx.doi.org/10.21622/RESD.2026.12.1.1889

[22], 2025	To design an intelligent control system for solar-powered EV charging stations to enhance energy production.	ANN-based MPPT comparing three training architectures: LM, SCG, and BR.	PV system integrated with a wireless charging station infrastructure for EVs.	MATLAB/ Simulink.	Coordinated energy flow from PV to the EV battery through an intelligent charging interface.	Variable environmental conditions (irradiation and temperature) affect power extraction.	Overall efficiency of the charging station, tracking speed, and steady-state oscillations.	-An SCG-based ANN is the most effective for dynamic performance, according to a comparative analysis of LM, SCG, and BR algorithms.
[23], 2026	Improve power quality and enhance MPPT efficiency in PV/wind hybrid microgrids.	Dual ANN-based control.	PV/wind hybrid system integrated with a unified power quality conditioner (UPQC).	MATLAB/ Simulink.	Coordinated control for voltage regulation and harmonic mitigation between PV/ wind and UPQC.	Unbalanced conditions, short-circuit faults, variable irradiance and temperature, load variations, nonlinear loads, and voltage sag/ swell (20%).	Power factor (≈1), response time, efficiency, MSE, and THD (voltage: 0.68 - 0.70%; current: 1.68 - 1.73%).	-Integrated ANN-MPPT with ANN-based UPQC under dynamic conditions.
[24], 2026	To use DC link behavior properties to improve MPPT efficiency and lessen oscillations in hybrid PV/ wind systems.	The ANN parameters were tuned by particle swarm optimization (hybrid PSO-ANN controller).	Hybrid PV/ wind with a DC link and battery storage.	MATLAB/ Simulink.	Without voltage or current sensors, an integrated MPPT supervisor manages both sources concurrently.	Variable in wind speeds and partial shading of PV modules.	DC link voltage ripple reduction, MPPT efficiency, and THE (Current: 3%, Voltage: 2%).	-Without the use of conventional feedback control sensors. -Sensorless MPPT supervision reacts to wind and shade variations.
Proposed study	Design, control, and evaluate an HES grid-connected PV/ wind	IC and ANN approach for MPPT	HES grid-connected 150-kW hybrid PV/ wind energy system	MATLAB/ SIMULINK with validation based OPAL= RT 4512 HIL	Coordinated operation of PV and wind to meet grid needs and enhance performance.	Variable temperature, solar irradiation, and wind speed	Tracking efficiency, MSE, RMSE, settling time	-MPPT- based ANN. -Validate through experimental HIL technique. -Improved power quality and efficiency, reduced power losses.

III. System description

A crossbred PV/wind power system that is grid-connected is depicted in Fig. 2. It consists of a grid-tied three-phase inverter, a three-phase step-up transformer, a DC/DC converter, a PV and wind power system, and a DC link. This paper proposes to control the MPPT using the IC, ANN, and ANFIS techniques and the inverter control using the FOPID control. A permanent magnet synchronous generator (PMSG) and a rectifier are also included in the wind generator to control the wind energy using the ANN technique and convert AC to DC. Moreover, to mitigate current harmonics at the inverter output and inject the grid-tied high-quality current, the 3-phase inverter is connected via an RL filter; the algorithms' results provide values for power, voltage, and current [25].

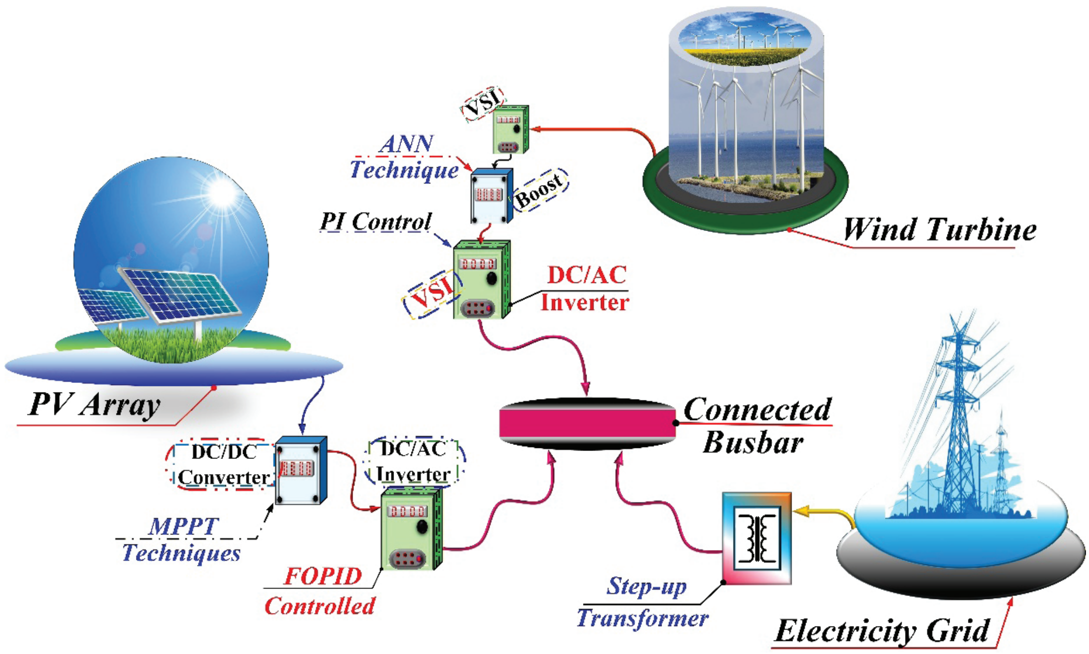

Figure 2: A PV/wind hybrid system for producing renewable energy.

A. *Mathematical modeling of PV cells*

A PV cell electric circuit modeling input is used to estimate a PV cell's output power, as demonstrated in Fig. 3. So, an integral ingredient of the design and analysis for PV control systems is the arithmetic modeling procedure of PV cells. Likewise, the relationship between the PV cell's current and voltage is described by equations that define the mathematical model for PV [26].

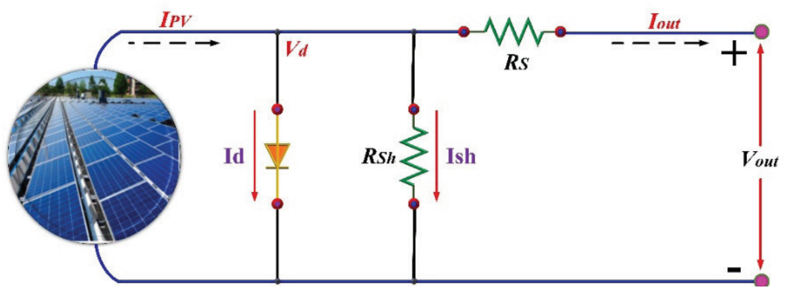

Figure 3: Circuit diagram for a solar PV cell.

$$I_{PV} = I_d + I_{sh} + I_o \tag{1}$$

$$I = I_{PV} - I_O\left\{e^{\left[\frac{q}{A*K*T*n_S}*(V+I*R_S*n_S)\right]} - 1\right\} \tag{2}$$

$$V = \frac{A*K*T*n_S}{q}\ln\left(\frac{I_{PV}+I_O-I}{I_O}\right) - I*R_S*n_S \tag{3}$$

The PV model uses key parameters to determine the I–V curve: Whereas I symbolizes the current that a PV module produces, I_{PV} is the PV cells inside produced current, I_d the diode reverse saturation current, R_S is the resistance of series, which has a very low value, R_P is a high value for the equivalent shunt resistance, A the factor of ideality, K the steady for Boltzmann, T is the temperature by Kelvin, and q the charge of electron.

B. *DC-DC converter model*

To optimize when the output voltage of a PV system is small, raise the voltage using the boost converter in the detailed model from 273.5 V to 500 V, as illustrated in Fig. 4. However, a DC/AC inverter is used to coordinate the voltage level with the electrical grid, and the DC/DC boost converter is used to increase the PV output voltage to achieve the desired voltage. So, adjust the duty cycle using the following equation [27]:

Volume 12, Issue 1, June 2026 - ISSN 2356-8569
http://dx.doi.org/10.21622/RESD.2026.12.1.1889

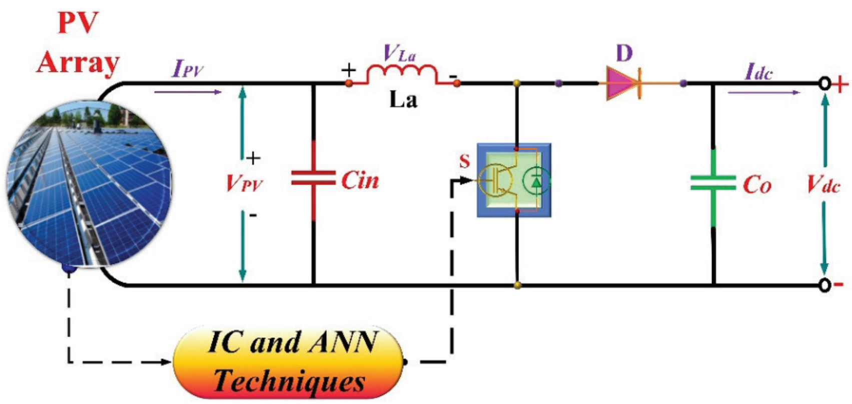

Figure 4: Basic configuration of boost converter.

$$V_{OUT} = \frac{V_{IN}}{1-D} \quad (4)$$

C. Wind Turbine

By the wind turbines' (WT) blades, the wind turbines' kinetic power is converted into mechanical power. Where the PMSG is primarily used in small-scale generating systems, especially wind energy setups [12, 28]. So, the PMSG functions effectively without requiring an external excitation circuit for DC power, as displayed in Fig. 5. Thus, the grid-side converter (GSC) controls the active power of the grid-side *dq-axis* currents. Consequently, the DC-Link voltage of the machine-side converter (MSC) maximizes the wind power of machine-side *dq-axis* extraction by optimizing PMSG speed. Whereas the DC-Link acts as a buffer, power imbalances among the converters cause voltage fluctuations [28, 29].

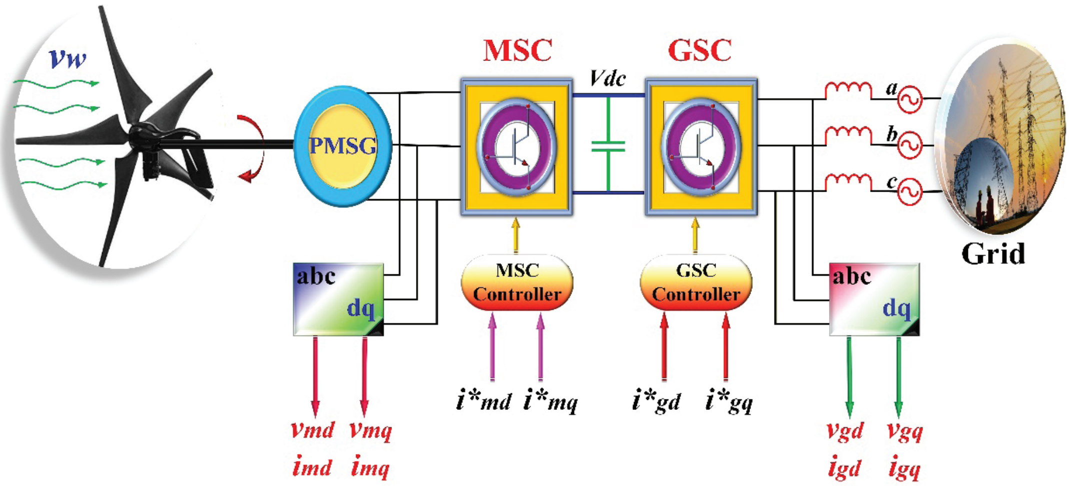

Figure 5: Schematic representation of PMSG-based wind turbine.

While it boasts a strong power-to-weight ratio, its performance is constrained by the high cost of permanent magnets and reduced magnetic strength at high temperatures. So, quantify the aerodynamic energy extracted by a rotating turbine blade; the next mathematical model can be completed [13, 29].

$$P_{\omega} = \frac{1}{2}\rho A C_p(\beta * \lambda) V_{\omega}^3 \quad (5)$$

$$T_{\omega} = \frac{1}{2}\rho \pi R^3 V_{\omega}^2 * \frac{C_p(\beta * \lambda)}{\lambda} \quad (6)$$

Where:- P_{ω} is symbolizes the power that a wind turbine produces, ρ is the density of air by (k/m^3), and A the rotating blades of area covered, C_p is represents a wind turbines performance coefficient according to the rotor throw angle β (*in degrees*), and V_{ω} perform a speed of wind (*m/s*), λ is determined by a ratio of tip speed for turbine, ω_r is represents a speed of rotor (*rad/s*), R is radius of the wind turbine rotor (*m*), and T_{ω} corresponds to the output torque.

Volume 12, Issue 1, June 2026 - ISSN 2356-8569
http://dx.doi.org/10.21622/RESD.2026.12.1.1889

D. Voltage source inverter controller

The PV station is connected to a point of common coupling (PCC) busbar via a three-level modulation of pulse width (PWM) inverter of three phases, as depicted in Fig. 6. The voltage source inverter (VSI) is controlled. A control system maintains a constant DC-link voltage between the VSI control and DC/DC converter while controlling a PV array to inject the reactive power [30]. Thus, a current controller of the decoupled loop for the phase-locked loop (PLL) and a controller of the DC-link voltage are the three most crucial components of the VSI controller. It is used to keep the DC-link condenser voltage at a fixed value of 500 V [31]. Furthermore, the inverter output current must be converted to the active current (I_d) and reactive current (I_q) ingredients, respectively, in order to operate a second control circuit, a controller for the current. Therefore, the VSI control strategy's PI and FOPID controller setting parameters are given. The following features of the voltage and current controller for the DC-link can be characterized [11, 32]:

$$I_{d\_ref} = K_{p_1}(V_{dc1\_ref} - V_{dc1}) + K_{i\_1}\int(V_{dc1_{ref}} - V_{dc1})dt \quad (7)$$

The proportional-integral (PI) controller is a simplified version of the proportional–integral–derivative (PID) controller that combines proportional gain K_p and integral gain K_i without a derivative term. Its main topic is to remove the steady-state inaccuracy and improve output accuracy, although it may lead to a longer response time compared to PID in fast systems. While PI and PID controllers are widely used in dynamic system control due to their simplicity and effectiveness, their performance can be limited when dealing with complex or nonlinear systems because they rely only on integer orders for integration and differentiation [33]. Where the equations provided are used to calculate the proportional (K_p) and integral (K_i) gains for a controller [11]:

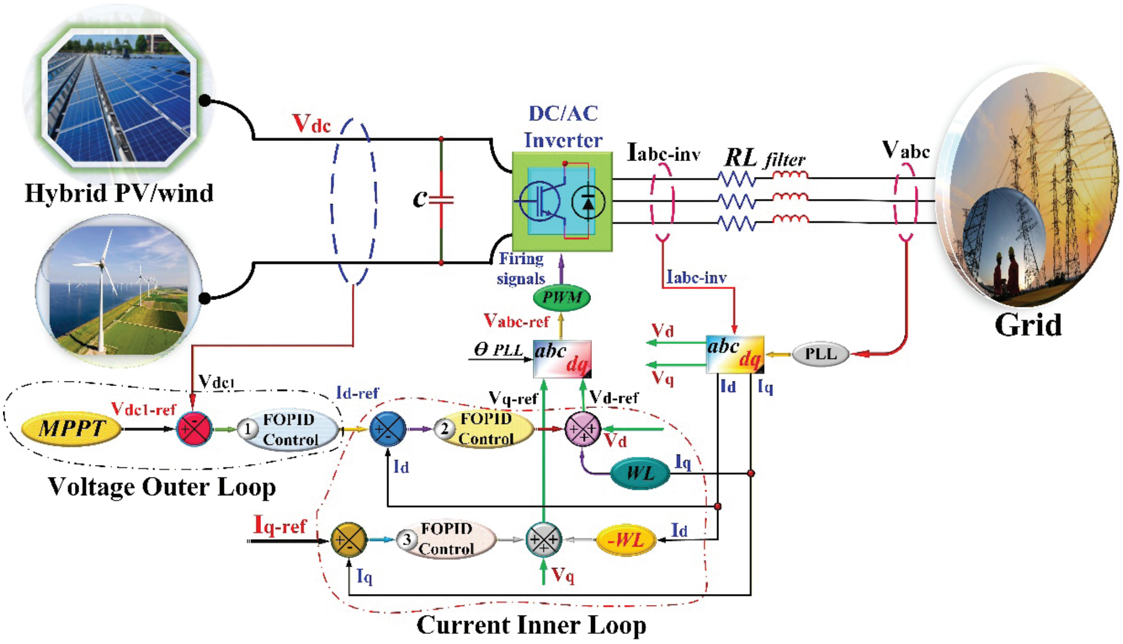

Figure 6: Control strategy of the DC/AC Inverter.

$$K_{p(2,3)} = \frac{L_f}{t_{pwm}} \quad (8)$$

$$K_{i(2,3)} = \frac{R_f}{t_{pwm}} \quad (9)$$

Where:- K_p is the proportional gain based on the connection between the inductance and the PWM time period, K_i is the integral gain using the resistance and the PWM time period, L_f is the inductance for the filter, R_f is the resistance for the filter, and t_{pwm} is the PWM time period.

The FOPID is a well-known example of the more flexible and accurate controllers that have been made possible by this limitation, which has prompted researchers to create control concepts based on fractional derivatives and integrals [33]. In contrast, the tools needed to control dynamic systems must be able to balance stability, accuracy, and response time. Whereas since FOPID permits λ and μ to be positive real values between 0 and 1, it offers more flexibility in tuning and controlling system responses than the traditional PID, which uses first-order integration (λ ≤ 1) and first-order

http://dx.doi.org/10.21622/RESD.2026.12.1.1889

differentiation ($\mu \leq 1$). Therefore, its equation is given as in Eq. (10) [34]:

$$C_{(t)} = k_p + \frac{k_i}{s^{\lambda}} + k_d * s^{\mu} \quad (10)$$

Where: K_p, K_i, and K_d stand for proportional, integral, and derivative gains, respectively. It is perfect for nonlinear or dynamically complex systems that are difficult to tune with conventional PI controllers because of its flexibility, which allows for a better balance between quick response, fewer oscillations, and increased stability. The FOPID is proposed to control the inverter in the hybrid system based on trial and error methods for tuning the coefficients of the fractional controller. After a deep study of the system, the chosen parameters for the FOPID are 7, 800, 0.10108, 0.89, and 0.44 for K_p, K_i, K_d, λ, and μ, respectively.

IV. Proposed methodology

A. Incremental conductance technique

In a PV/wind system connected to the grid, one of the most popular and successful MPPT strategies is the IC technique. Where the underlying idea is that at the MPP, the power derivative to the rating of voltage is zero [11]. Also, the algorithm defines the direction of operating voltage regulation by calculating the instantaneous conductance (*I/V*) and the IC technique (*dI/dV*) from the system's real-time current and voltage volumes. When the two values are equal, the system is functioning at its best; when the difference is either positive or negative, the voltage is changed to get closer to that point [24]. Consequently, the IC algorithm is proposed in many studies to extract the maximum power from the PV system and maintain a high value of overall efficiency for the system in situations of variations in environmental conditions. The mathematical description for the IC is depicted in the following equations:

$$\frac{dI}{dV} > -\frac{Ipv}{Vpv} \quad \text{If the left MPP} \quad (11)$$

$$\frac{dI}{dV} < -\frac{Ipv}{Vpv} \quad \text{If the Right MPP} \quad (12)$$

$$\frac{dI}{dV} = -\frac{Ipv}{Vpv} \quad \text{At the MPP} \quad (13)$$

As discussed, the IC technique can quickly adjust the deviation of power from the maximum power point in case of changes in temperature and solar irradiation, in contrast to the P & O algorithm [35]. However, in computational complexity, the requirement for exact measurements and the algorithm's vulnerability to signal noise are considered the most significant disadvantages for this technique, which can cause an accuracy loss with significant fluctuations [36]. Fig. 7 demonstrates the flowchart of the IC algorithm.

Figure 7: IC algorithm flowchart.

B. Artificial neural network technique

A grid-tied PV/wind crossbred system's performance can be evaluated and predicted using the ANN technique, which offers a flexible and adaptable framework. The ANN technique is a useful method for learning complex relationships between various operational parameters and forecasting the overall behavior of a system [34]. Because the neural network is trained on data, it can recognize and generalize patterns in a wide range of scenarios. In addition, under a range of environmental conditions, including fluctuating wind speed and PV irradiance, the trained ANN model can accurately predict critical performance parameters like output power, voltage, and current [37]. In this work, the proposed strategy utilizes MPPT technology based on ANN, trained employing data collected and captured from an algorithm of IC, to improve the performance of PV systems in HES. Recent studies on the operation of microgrid, smart renewable energy management, hybrid microgrid optimization, and neural control approve the effectiveness of intelligent methods, optimization techniques, and ANN-based techniques in modern applications of renewable energy [38-41].

The ANNs are particularly well-suited for creating renewable energy techniques and managing the operational challenges of grid-connected PV/wind crossbred systems because of their generality and strong generalization ability [42]. The considered ANN is selected to be a feedforward neural network including three distinct layers: an output layer, an input layer, and two hidden layers. The layer of input includes 6 inputs representing the PV power, delayed power with one sample, current, current with delayed one sample, voltage, and voltage with delayed one sample signals, while the hidden layer consists of one hidden layer with 15 neurons. The output layer includes one neuron that generates the optimal duty cycle for the control process of the converter for MPPT. The activation functions used for this network for the hidden layer and output layer are tansig and purelin functions, respectively. The network is trained using the Scaled Conjugate Gradient backpropagation method with a learning rate of about 0.01. The training process was conducted for a number of epochs, about 1000 epochs, with a target value of MSE around 10^{-5} as the stopping criterion. Furthermore, an early stopping process is applied based on the performance of validation to avoid overfitting. Furthermore, Fig. 8 illustrates how the layers regulate the processing and output transformation of incoming data [43]. Continuing this analysis, Fig. 9 illustrates the suggested ANN algorithms flowchart for MATLAB/Simulink MPPT technology implementation [44]. Moreover, the accuracy of the improved strategy is evaluated using Integral of Time Absolute Error (ITAE), Root Mean Squared Error (RMSE), and Mean Squared Error (MSE) as in the following equations [34, 45, 46,47]. Besides, the tracking error and efficiency are also used in the evaluation process in this paper, as in Eqs. (17) and (18) [47]. Another formula for the efficiency of MPPT is also given in the evaluation as in Eq. (19).

$$\text{ITAE} = \int_0^T t\left|y_{actual}(t) - y_{predicted}(t)\right| dt \quad (14)$$

$$\text{MSE} = \frac{\sum_{i=1}^{n}(y_{actual} - y_{predicted})^2}{n} \quad (15)$$

Where: n is the sampling size, T is the time, y_{actual} is the true values, and $y_{predicted}$ is the predicted values.

$$\text{RMSE} = \sqrt{\frac{1}{n}\sum_{i=1}^{n}(y_{actual} - y_{predicted})^2} \quad (16)$$

$$\text{Tracking Efficiency (\%)} = \frac{P_{PV}}{P_{MMP}} \times 100 \quad (17)$$

$$\text{Tracking Error (\%)} = \frac{P_{MMP} - P_{PV}}{P_{MMP}} \times 100 \quad (18)$$

$$\eta_{MPPT} = \frac{\int P_{measured}(t)dt}{\int P_{ideal\,MPP}(t)dt} \quad (19)$$

Volume 12, Issue 1, June 2026 - ISSN 2356-8569
http://dx.doi.org/10.21622/RESD.2026.12.1.1889

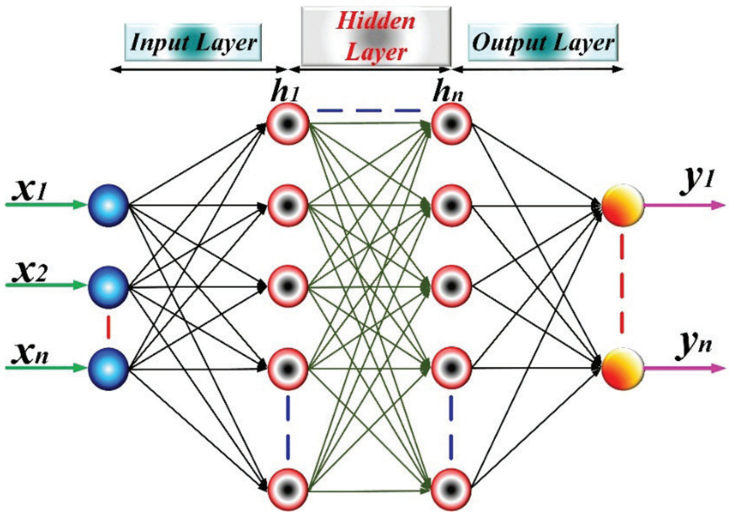

Figure 8: Schematic representation of the ANN.

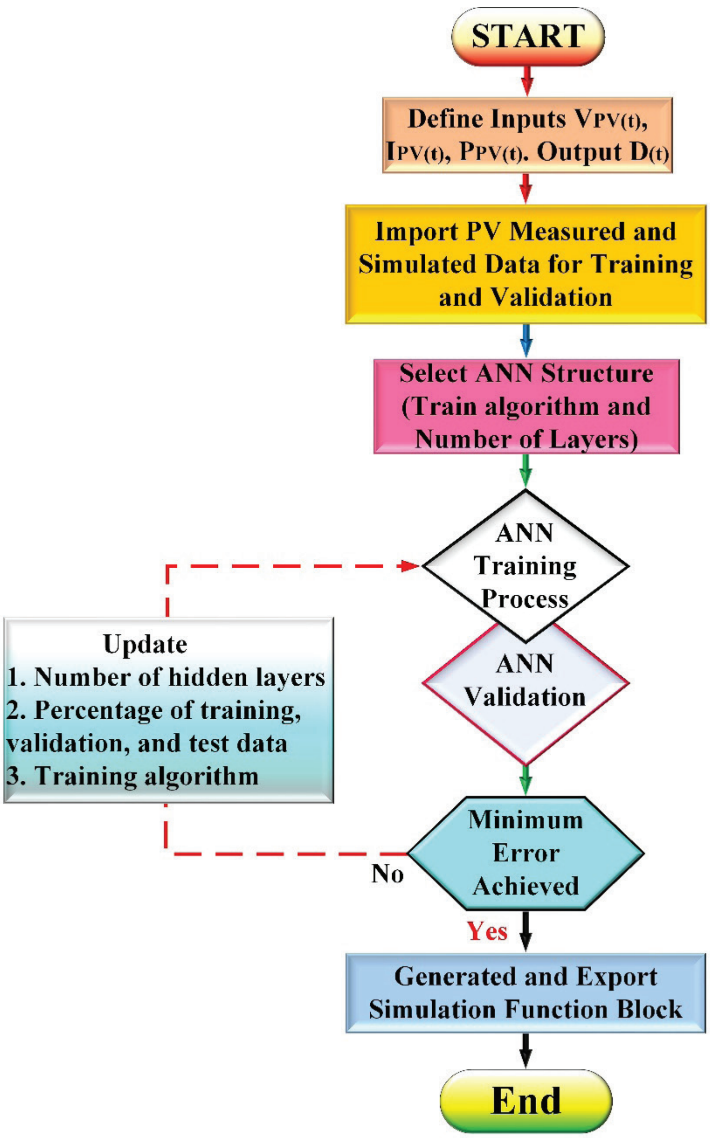

Figure 9: A flowchart of the ANN technique.

V. Experimental system

To validate and test control strategies in real time under various operating conditions, the experimental system in this study is made to seamlessly interface with the OPAL-RT 4512 platform. Furthermore, the platform offers adaptable analog and digital I/O interfaces that facilitate integration with real or semi-real power systems, supports a range of simulation tools such as MATLAB/Simulink and RT-LAB, and allows control devices such as MPPT controllers or inverters to be accurately and safely tested before being used in real-world applications [48].

The OPAL-RT 4512 is used to assess how well renewable power systems perform under dynamic and quickly changing conditions, such as variations in wind speed or solar irradiation. Quick system response evaluation and appropriate control strategy modification are made possible by this real-time feature. Moreover, the platform simulates real-world systems, maintaining the temporal accuracy of the real processes while allowing researchers to create and evaluate intelligent algorithms like AI-based controllers or machine learning techniques. So, this type of real-time simulation also offers a safer and more economical method of verifying cutting-edge energy technologies, enhancing grid stability and operational effectiveness [49]. In addition, using the RT-LAB environment platform, Fig. 10 shows how to integrate a Simulink-generated simulation model with the OPAL-RT 4512 real-time simulation.

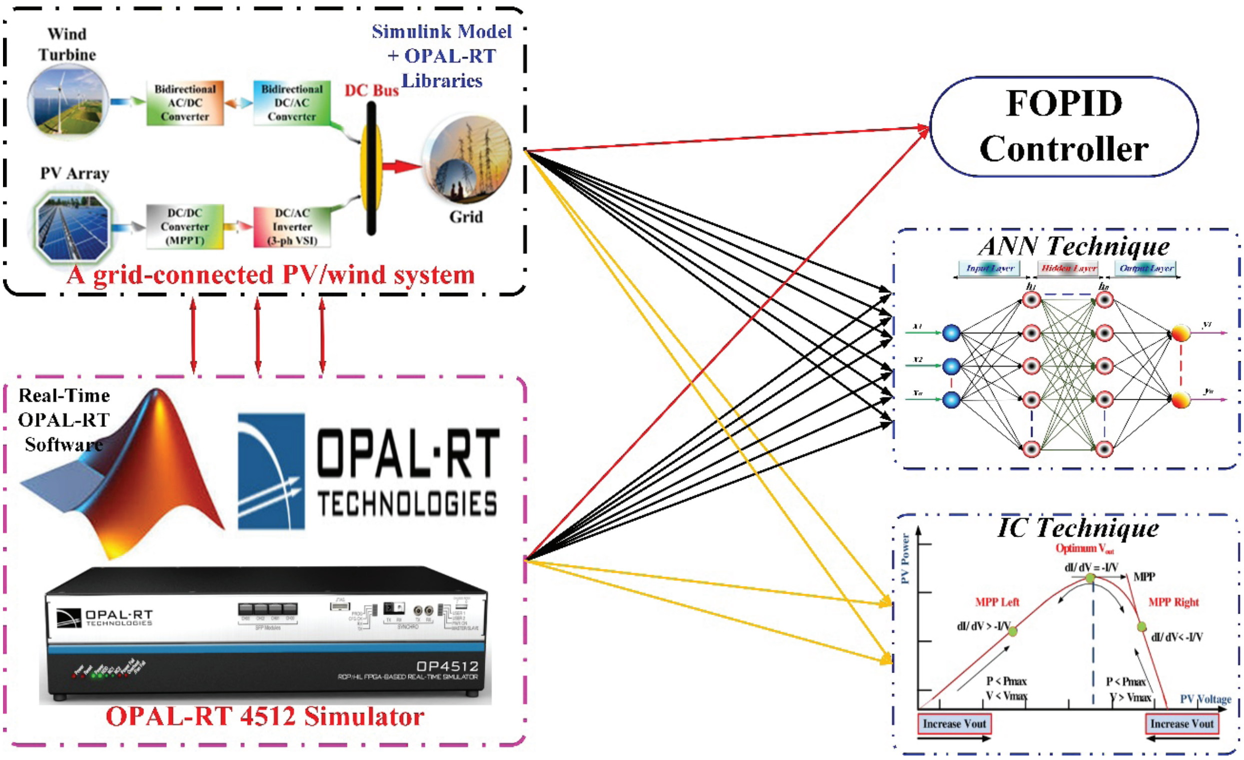

Figure 10: Grid-connected PV/wind power system simulation in Real-time with OPAL-RT.

VI. Results and Discussion

This section consists of MATLAB simulation result findings and experimental findings for OPAL-RT 4512 implementation. The operation is compared at various operating conditions to highlight the validation of the techniques used; comparisons are made to ensure accuracy, reliability, and usability of the developed model.

A. Weather conditions of the PV and wind system

Fig. 11a presents the step-changing profile of solar radiation with time variation, while Fig. 11b presents the temperature profile. Moreover, Fig. 12 presents the special pattern of wind speed variation throughout the simulation. Additionally, Table 2 details the specifications of the PV/wind system and grid; all components of the simulation and experimental system are explained in the results section.

 Volume 12, Issue 1, June 2026 - ISSN 2356-8569
http://dx.doi.org/10.21622/RESD.2026.12.1.1889

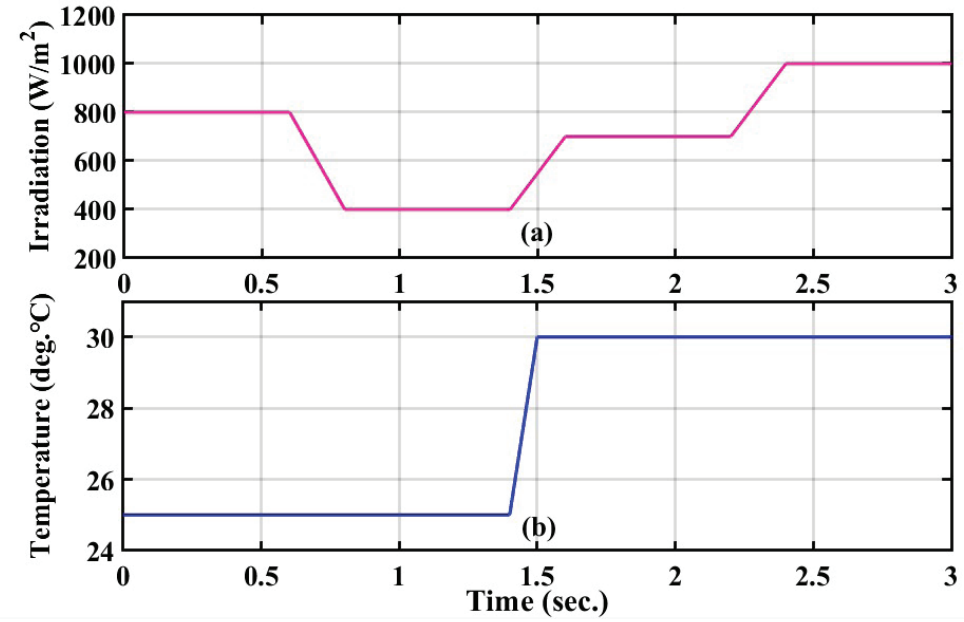

Figure 11: (a) Radiation changes. (b) The PV arrays temperature variations.

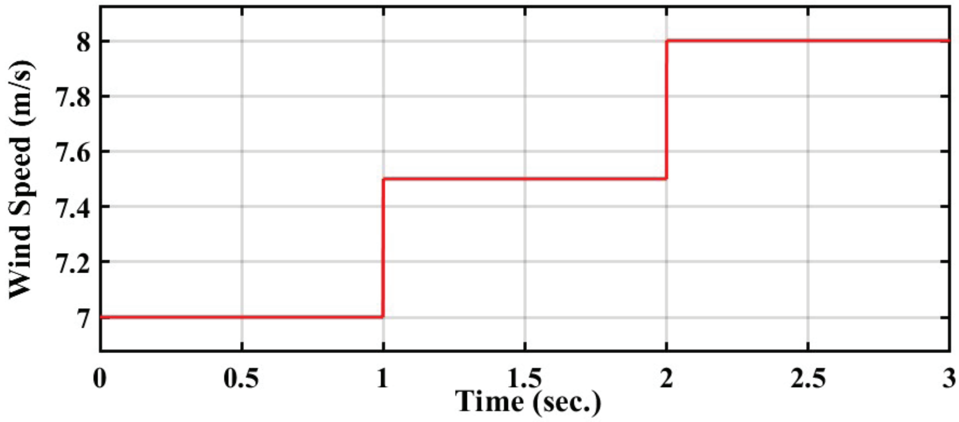

Figure 12: Changes in wind speed.

Table 2: Specification of the description system

Parameters for System	Values
Specifications of the PV system	
A PV Array	100.7 KW
A PV Module	305.23 W
In parallel strings	66
In a series string	5
Converter inductance	5×10^{-3} H
Converter impedance	0.005 Ω
Capacity of converter	100×10^{-6} F
Specifications of the wind system	
Rectifier impedance	100 Ω
Rectifier capacitor	0.1×10^{-6} F
Wind power	50 KW
Specifications of grid-tied	
Transformer step up	270 V/25 KV
Voltage of the grid	20,000 V
Frequency of the grid	60 Hz
Grid-tied with PV/wind	150 Kw

B. *Performance analysis of PV system MPPT techniques*

The voltage response of the PV system under different MPPT control strategies for simulation and experimental results is demonstrated in Fig. 13. In the time interval 0 to 0.4 s, the IC technique shows a sharp drop to approximately 125 V, whereas the ANN technique maintains voltage levels closer to the upper operational range of 250 to 275 V, indicating better voltage stability. Moreover, the ANN technique provides the most accurate and stable voltage tracking, where it minimizes oscillation and maintains a voltage that is closest to the reference (273.5 V).

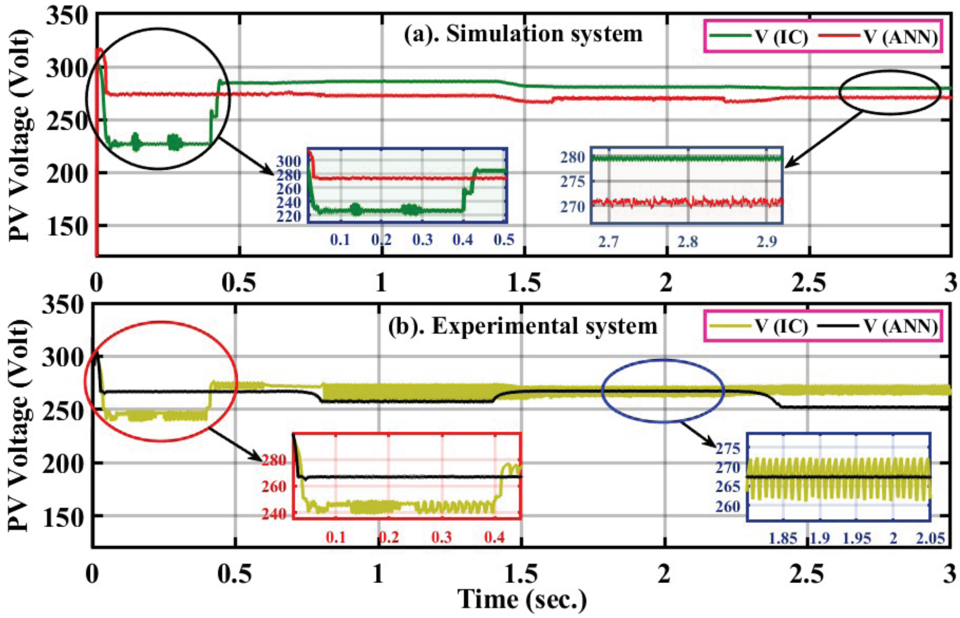

Figure 13: Comparison of PV voltage for (a). Simulation system (b). Experimental system.

The PV array current variation under the effect of MPPT techniques for simulation and experimental results is depicted in Fig. 14. The IC technique presents unstable tracking with sharp current dips. While the ANN technique tracks the changes more effectively, it shows mild oscillations. In addition, the ANN technique demonstrates superior performance, maintaining current levels with high stability and fast adaptation during irradiance variations. So, the simulation results were compared to experimental system data; they showed a high degree of agreement, indicating that the ANN approach offers superior dynamic tracking and current control.

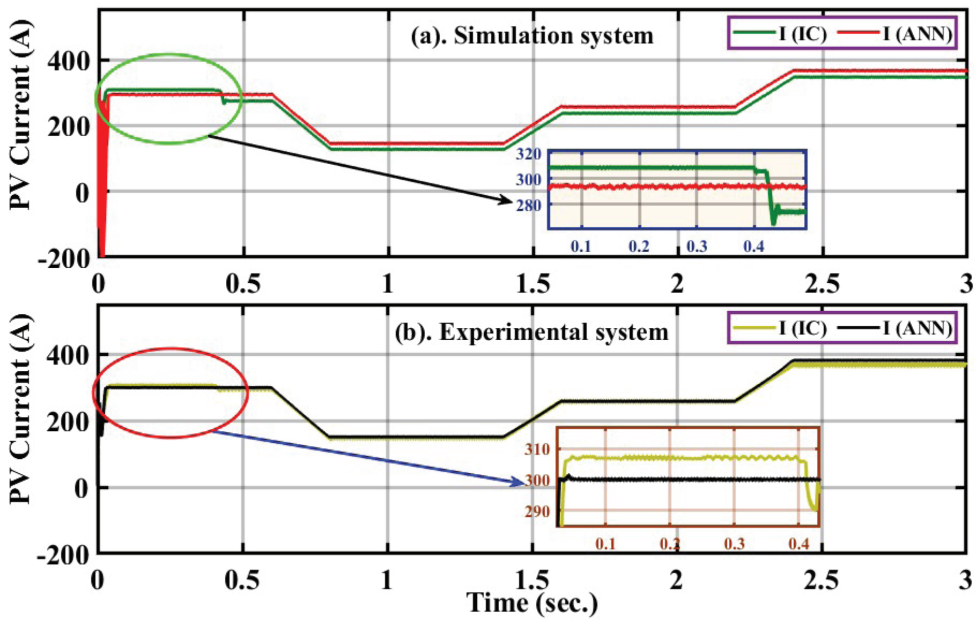

Figure 14: Comparison of PV current for (a). Simulation system (b). Experimental system.

Volume 12, Issue 1, June 2026 - ISSN 2356-8569
http://dx.doi.org/10.21622/RESD.2026.12.1.1889

The power output for the PV array under various MPPT technicalities of simulation and experimental results is displayed in Fig. 15, where the depicted IC technique shows inconsistent power tracking with clear drops during irradiation variations. While the ANN technique provides the most consistent output, closely following the expected irradiation profile, demonstrating better tracking accuracy and minimal fluctuation when compared to reference power, a decrease in value occurs at 2.4 s to the end of the period. At the same time, the power loss of the IC technique occurs between 0 and 0.5 s.

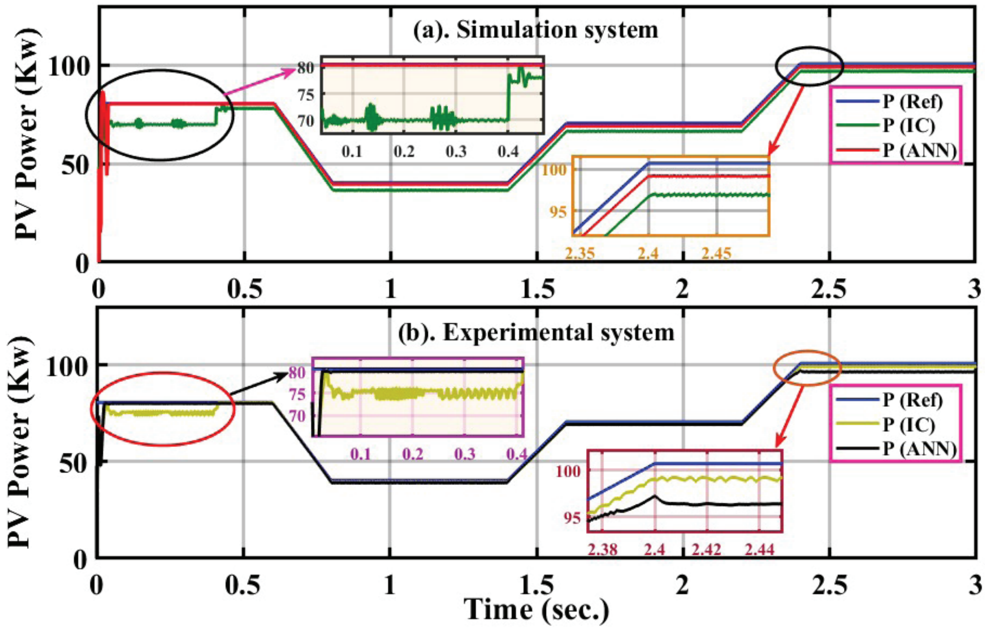

Figure 15: Comparison of PV power for (a). Simulation system (b). Experimental system.

Table 3 presents a numerical comparison of suggested MPPT techniques for simulation and experimental results under varying irradiation levels. Thus, readings of PV voltage, current, and output power at different times are included. The findings show that in both low and high irradiation conditions, the ANN technique consistently outperforms IC in terms of tracking stability and efficiency. Where the ANN technique is the best MPPT technique overall, according to the comparative data, it continuously produces the highest and most stable power output at all irradiance levels.

Table 3: PV performance results for the experimental and simulation systems are compared

MPPT Technique	Irradiation (W/m²)	Times (s)	V_{PV} (V)		I_{PV} (A)		P_{PV} (Kw)	
			Simulink	Experimental	Simulink	Experimental	Simulink	Experimental
IC	800	0.2	226.65	246.6	308.425	306.75	69.93	75.6
		0.5	284.37	274.43	247.1	293.18	78.17	80.415
	400	0.9	285.897	268.63	127.51	148.14	36.55	39.064
		1.4	286.12	270	127.45	147.41	36.45	39.16
ANN	800	0.2	273.3	266.874	294.38	300.22	80.452	80.045
		0.5	273.08	267.123	294.65	300	80.453	80.178
	400	0.9	271.95	258.015	145.55	151.5	39.624	39.125
		1.4	272.75	257.112	145.48	151.76	39.58	39.075

Volume 12, Issue 1, June 2026 - ISSN 2356-8569
http://dx.doi.org/10.21622/RESD.2026.12.1.1889

Table 4 shows the performance comparison of MPPT techniques for simulation and experimental results under various temperature and irradiance scenarios. According to the results, the ANN technique consistently outperforms the other method, achieving the highest MPPT efficiency and the lowest errors across all metrics, including MSE, RMSE, and ITAE. Additionally, the ANN method exhibits low efficiency and low mean squared errors, especially at low irradiance levels. On the other hand, the IC method exhibits lower MPPT efficiency and higher error rates, particularly when irradiance fluctuates, whereas efficiency declines and error rates rise with temperature. Furthermore, the MPPT efficiency is compared between simulation and experimental systems as shown in Table 5, where the ANN technique consistently outperforms the conventional IC technique, reaching a peak experimental efficiency of 97.43% and a simulation efficiency of about 96.80%.

Table 4: Performance of MPPT techniques based on efficiency and error analysis for simulation and experimental systems

Techniques	Irradiation (W/m^2)	Time (s)	Efficiency MPPT %		Error MPPT %		MSE Error		RMSE Error		ITAE Error	
			Simulation	Experimental	Simulation	Experimental	Simulation	Experimental	Simulation	Experimental	Simulation	Experimental
IC	800	0.4	86.9	94.48	13.1	5.52	10.1	22.24	9.98	3.87	0.8	0.394
	400	1	90.65	98.34	9.23	1.66	12.2	0.3	3.432	0.38	1.995	0.563
ANN	800	0.4	99	99.34	0.963	0.66	0.05	0.0024	0.2	0.045	0.0305	0.009
	400	1	95.93	97	4.065	3.01	1.93	0.93	1.35	0.926	0.405	0.212

Table 5: Efficiency of MPPT techniques for simulation and experimental systems

Techniques	η_{MPPT}	
	Simulink	Experimental
IC	92.97	97.32
ANN	96.80	97.43

C. *Performance analysis of wind turbine energy conversion system under different MPPT techniques*

The wind turbine generators' output current for MPPT suggested control strategies based on simulation and experimental results are shown in Fig. 16. The IC technique has a slow response and large current dips during transients according to the simulation and experimental results. In contrast, the ANN technique shows the most stable behavior, sustaining the current value with rapid settling and minimal deviation, suggesting superior adaptation to wind speed variables. Moreover, Fig. 17 illustrates how various MPPT techniques affect the wind turbine generators' active output energy for both simulation and experimental outcomes. Whereas the IC technique shows a slow response and lower power levels. Similarly, the ANN technique yields the most consistent results, peaking at about 5×10^4 watts with little ripple.

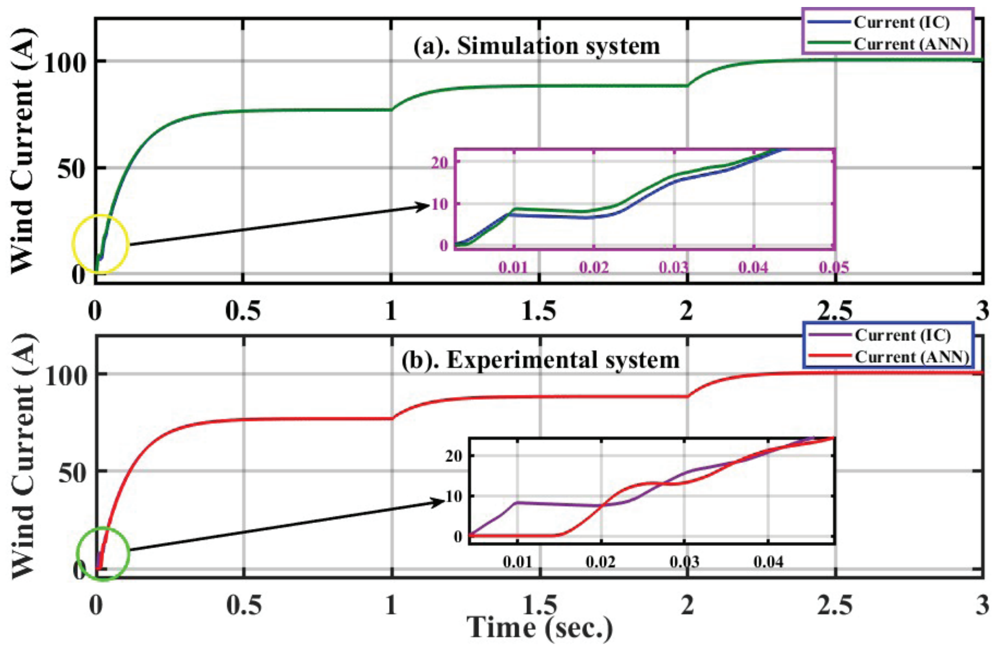

Figure 16: Evaluation of wind output current for (a). Simulation system (b). Experimental system.

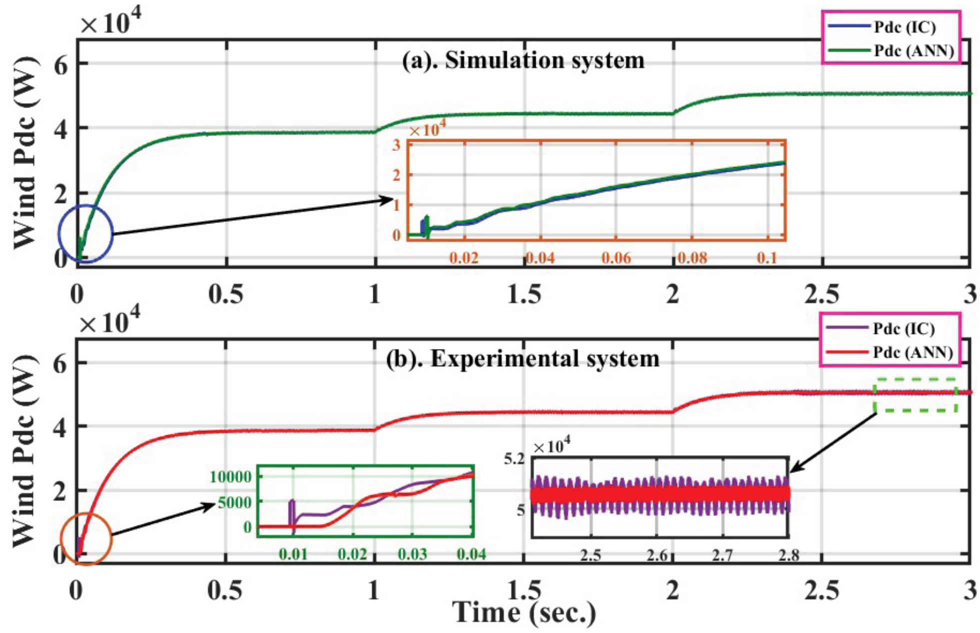

Figure 17: Evaluation of wind P_{dc} for (a). Simulation system (b). Experimental system.

The simulation and experimental results for the DC output voltage of the wind turbine power conversion systems are illustrated in Fig. 18. There is still some discernible ripple even though the IC technique improves voltage stability, especially during transients. The ANN method outperforms V_{Ref} by sustaining a constant voltage level of roughly 500 V_{dc}, indicating better energy regulation and more reliable converter behavior. Similarly, Fig. 19 shows each phase's instantaneous AC output power from the wind turbine generator using MPPT techniques in the simulation and experimental findings. While the ANN technique generates more reliable and stable three-phase power with distinct sinusoidal behavior and balanced phase characteristics, the IC technique shows notable imbalance and high ripple, indicating poor control and synchronization.

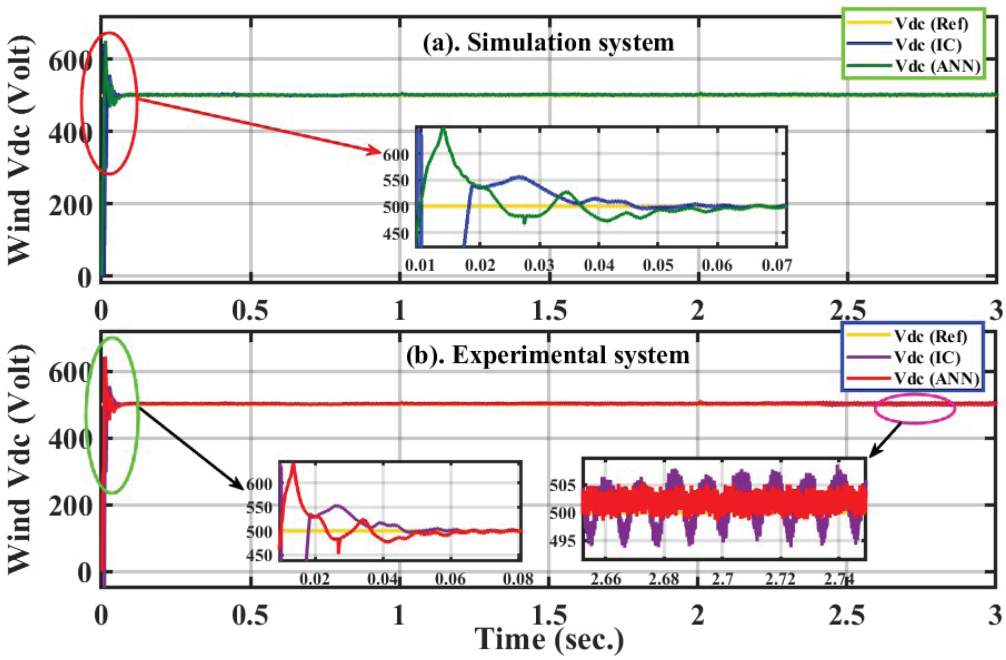

Figure 18: Wind DC voltage of the system for (a). Simulation system (b). Experimental system.

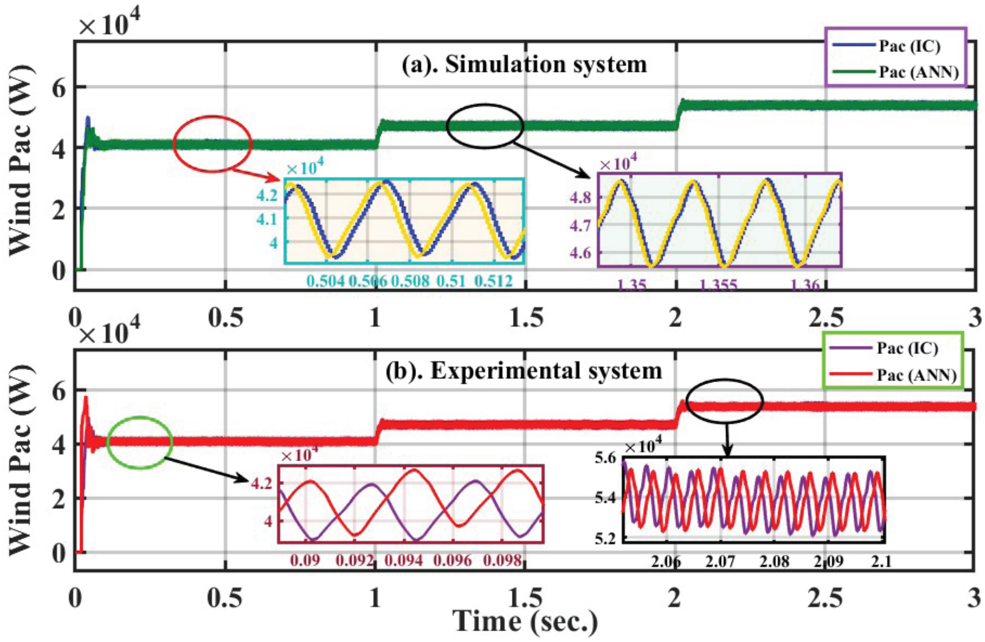

Figure 19: Analysis of the performance of P_{ac} for (a). Simulation system (b). Experimental system.

The rotor speed is a crucial mechanical component that demonstrates how well the turbine adapts to shifting wind conditions. Furthermore, Fig. 20 illustrates how different MPPT techniques affect the wind turbine rotor speed behavior in both simulation and experimental settings. The IC technique exhibits strong oscillations, delayed response, and unstable speed tracking when both simulation and experimental results are taken into account. The ANN technique, on the other hand, performs the most reliably, sustaining a speed of about 150 rad/s with little variation. A comparison of MPPT techniques applied to an experimental and simulation system is also shown in Table 6. It highlights the precision, stability, and effectiveness of each tracking method in dynamic wind conditions by examining rotor speed I_{dc} and P_{dc} at various wind speeds and times. Table 7 highlights how well the control process works with the following MPPT techniques: the results depict that the ANN presents distinct results in terms of settling time, overshoot, and rise time in comparison to the IC approach.

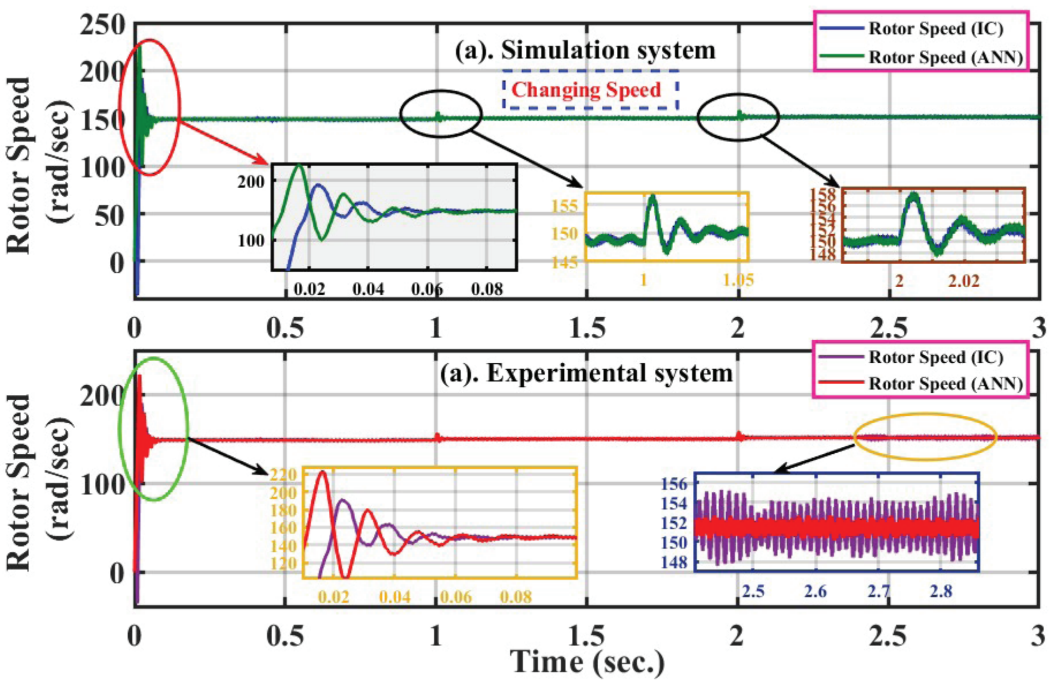

Figure 20: Rotor speed tracking performance of W/T for (a). Simulation system (b). Experimental system.

Table 6: Comparative evaluation of wind energy MPPT techniques for simulation and experimental systems

Techniques	Speed of Wind (m/s)	Time (s)	Speed of Rotor (rad/s)		I_{dc} Wind (Amp)		P_{dc} Wind (Watt)	
			Simulink	Experimental	Simulink	Experimental	Simulink	Experimental
IC	7.5	1.3	150.14	149.29	87.89	87.89	4.41 x 10^4	4.427 x 10^4
		1.8	149.005	149.94	88.48	88.47	4.443 x 10^4	4.426 x 10^4
ANN	7.5	1.3	149.54	149.33	87.89	87.9	4.417 x 10^4	4.417 x 10^4
		1.8	150.823	149.95	88.454	88.47	4.44 x 10^4	4.454 x 10^4

Table 7: Comprehensive performance analysis of MPPT techniques: time response for PV power, PV voltage, and DC-Link voltage stability under variable irradiation and temperature

Techniques Used	Irradiation & Temperature			Rise Time	Settling Time	Overshoot	Peak	Peak Time
IC	1000	25°C	P_{PV}	0.0214	NaN	0.0176	100.7377	0.4278
			V_{PV}	1.4263e-04	NaN	17.1202	320.3236	4.0000e-04
			V_{dc}	6.0655e-06	2.0088	32.1728	660.8638	0.0088
	400	25°C	P_{PV}	0.0026	NaN	0.0637	39.6953	0.4866
			V_{PV}	2.8655e-04	NaN	14.2478	307.6865	7.0000e-04
			V_{dc}	6.1585e-06	0.0410	30.1346	650.6731	0.0088
ANN	1000	25°C	P_{PV}	0.0347	0.0449	0	100.7004	0.0588
			V_{PV}	1.4603e-04	0.0476	17.0207	320.0515	4.0000e-04
			V_{dc}	0.0074	0.0469	27.7699	638.8497	0.0135
	400	25°C	P_{PV}	0.0024	0.0304	0.0177	39.6770	0.0668
			V_{PV}	2.9128e-04	0.0315	14.7969	309.1652	0.0137
			V_{dc}	0.0074	0.0463	25.9826	629.9128	0.0133

D. Performance analysis of grid-connected parameters under different MPPT techniques

The phase current (I_a) supplied to the grid behaved similarly for both the simulation and experimental results, as depicted in Fig. 21. The distorted waveform with observable harmonics is produced using an IC technique. Additionally, the ANN technique displays perfect performance with low ripple and enhances the waveform shape. Furthermore, at an irradiation of 1000 W/m^2, the ANN technique maintains a clean current oscillation around ±5 A, demonstrating the most sinusoidal and symmetrical waveform, indicating efficient current injection. Similarly, Fig. 22 depicts the simulation and experimental results for the grid phase voltage (V_a), where the voltage waveforms are compared during different techniques. The shape is improved by the IC technique, although there are some distortions and a small phase offset. In contrast, the ANN technique consistently produces smooth transitions, full voltage utilization, and low waveform distortion while maintaining a nearly perfect sinusoidal waveform with a stable peak amplitude around ±2×10^4V, exhibiting strong voltage regulation.

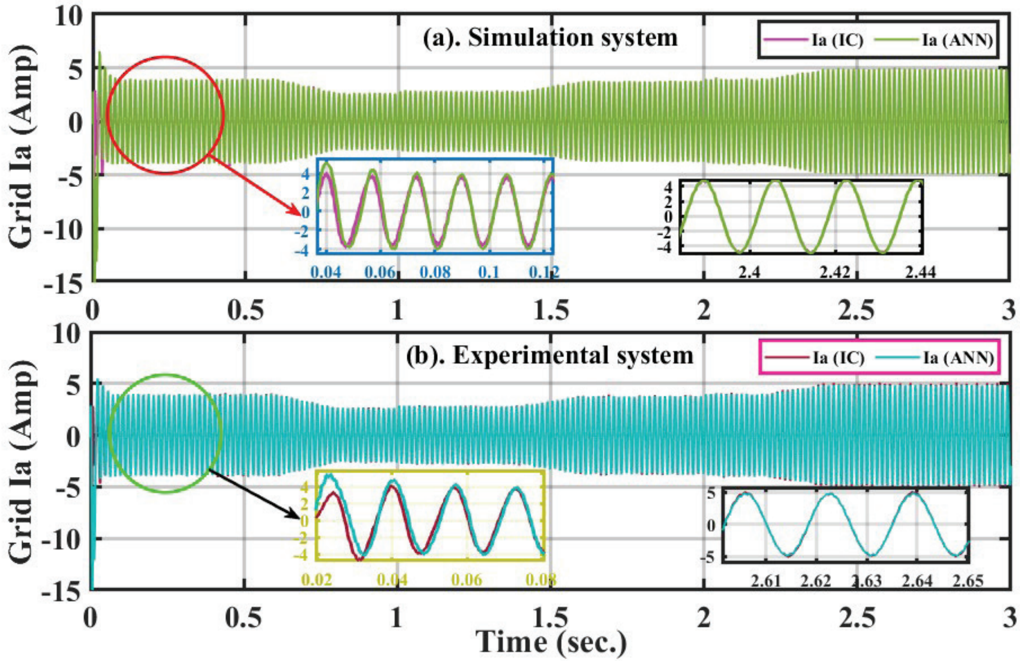

Figure 21: Grid phase current (I_a) response for (a). Simulation system (b). Experimental system.

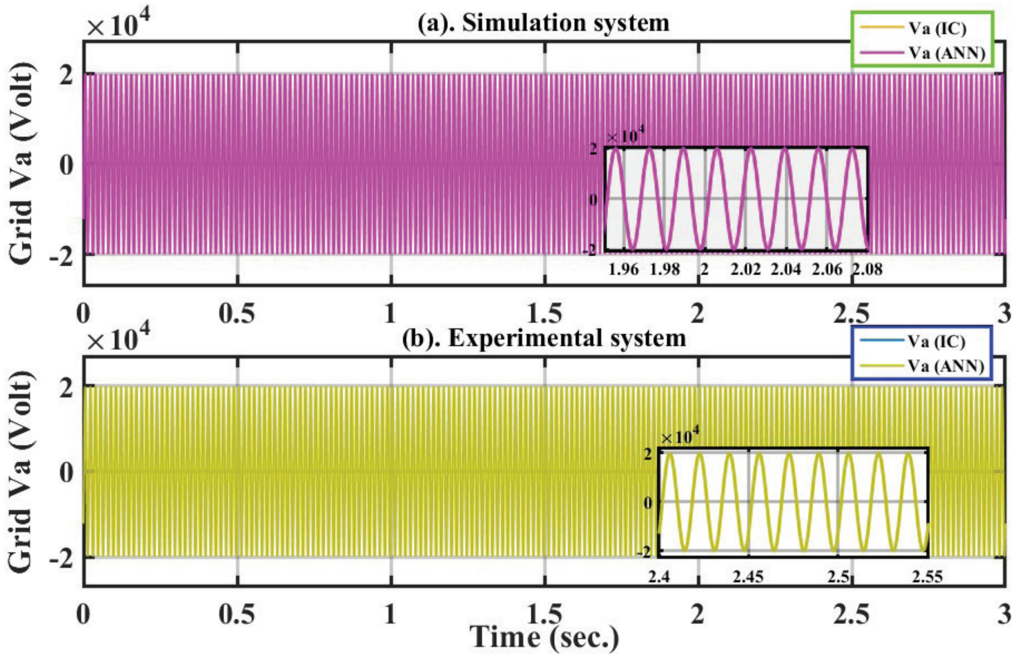

Figure 22: Grid phase voltage (V_a) response for (a). Simulation system (b). Experimental system.

The best performance is plotted in Fig. 23 with the ANN technique, where the currents closely follow the reference grid signals in simulation and experimental results. Increased MPPT responsiveness, better switching control, and efficient harmonic mitigation are all reflected in the waveform purity across all three phases. The distorted waveform with observable harmonics for an IC technique. Lastly, proving that the ANN technique is the most effective of the methods under comparison. As a result, once high interaction between simulation and experimental results was demonstrated, the analytical approach was built with confidence.

Volume 12, Issue 1, June 2026 - ISSN 2356-8569
http://dx.doi.org/10.21622/RESD.2026.12.1.1889

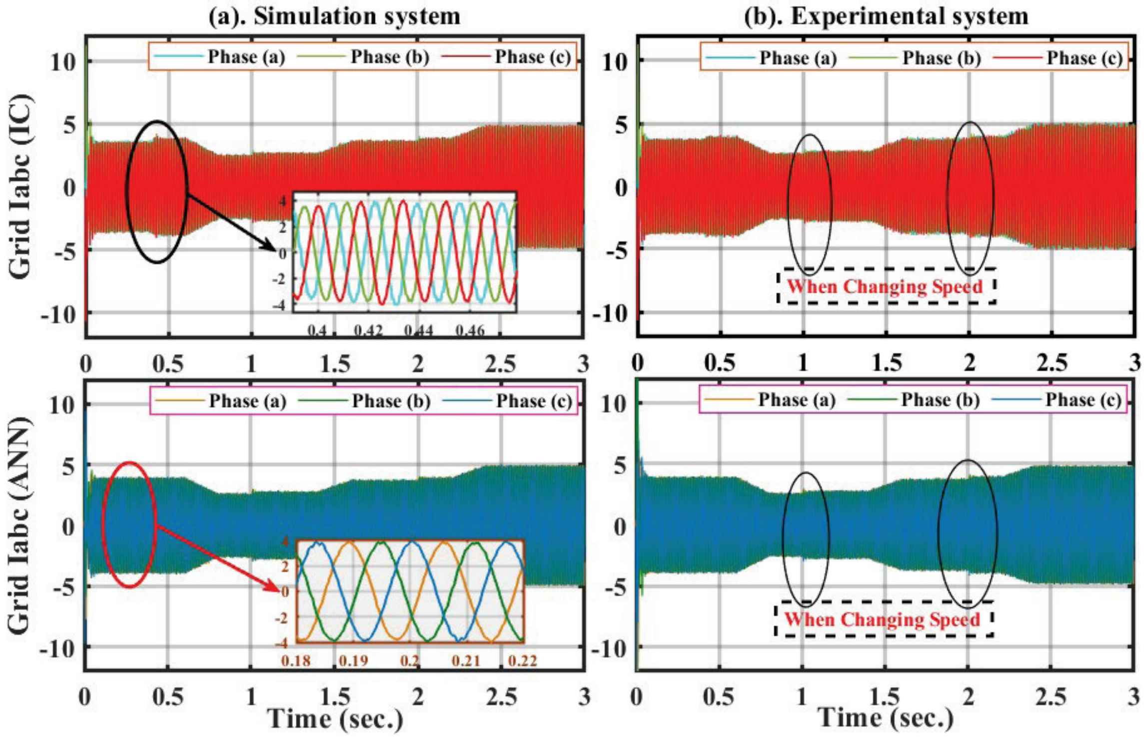

Figure 23: 3-Phase grid current performance of MPPT techniques for (a). Simulation system (b). Experimental system.

The superior performance of the ANN technique, where all three voltage phases show excellent synchronization and high-fidelity sinusoidal waves, is demonstrated in Fig. 24, where the simulation and experimental values maintain a nearly perfect sinusoidal waveform with a stable peak amplitude of about $\pm 2\times10^4$V, confirming perfect waveform alignment and minimal harmonic interference. The shape is improved by the IC technique, although there are some distortions and a small phase offset. Overall, it shows that the experimental setup effectively reflected the scenarios examined through simulation and that the ANN technique guarantees the highest voltage quality, supporting effective and safe power transfer in the hybrid renewable system.

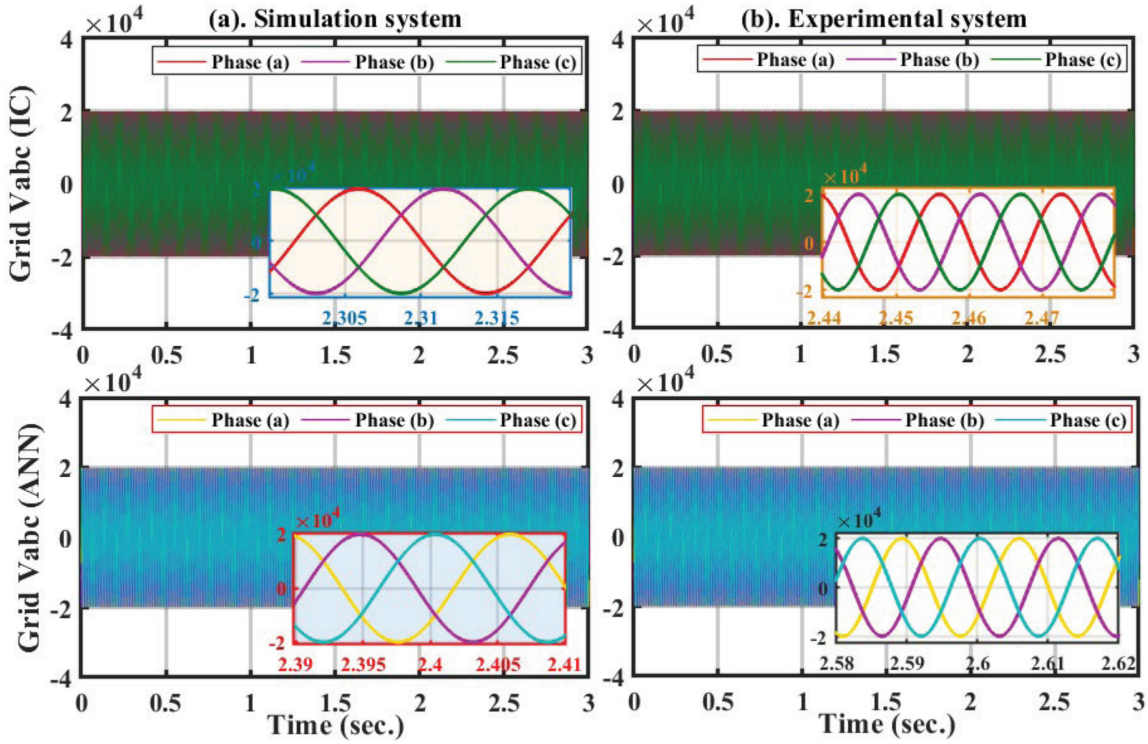

Figure 24: Performance 3-phase grid voltage of MPPT techniques for (a). Simulation system (b). Experimental system.

Volume 12, Issue 1, June 2026 - ISSN 2356-8569
http://dx.doi.org/10.21622/RESD.2026.12.1.1889

The crossbred system's overall output power into the grid-tied system from both wind and PV sources is displayed in Fig. 25, using different MPPT techniques based on simulation and experimental results. demonstrating that the ANN technique offers the best control performance, guaranteeing proportionality and the power for high-quality grid delivery tied to variable input from both PV and wind sources. Thus, the effectiveness of the design and modeling process was demonstrated by the system's actual implementation, which closely resembled the simulated behavior. Continuing this analysis, Table 8 presents a comprehensive comparison of MPPT techniques in a hybrid PV/wind system. In order to evaluate P_{PV}, P_{Wind}, P_{Total}, and P_{Grid}, it takes into account solar irradiation, wind speed, and time. Additionally, the goal is to evaluate overall energy delivery and tracking efficacy in a range of environmental circumstances.

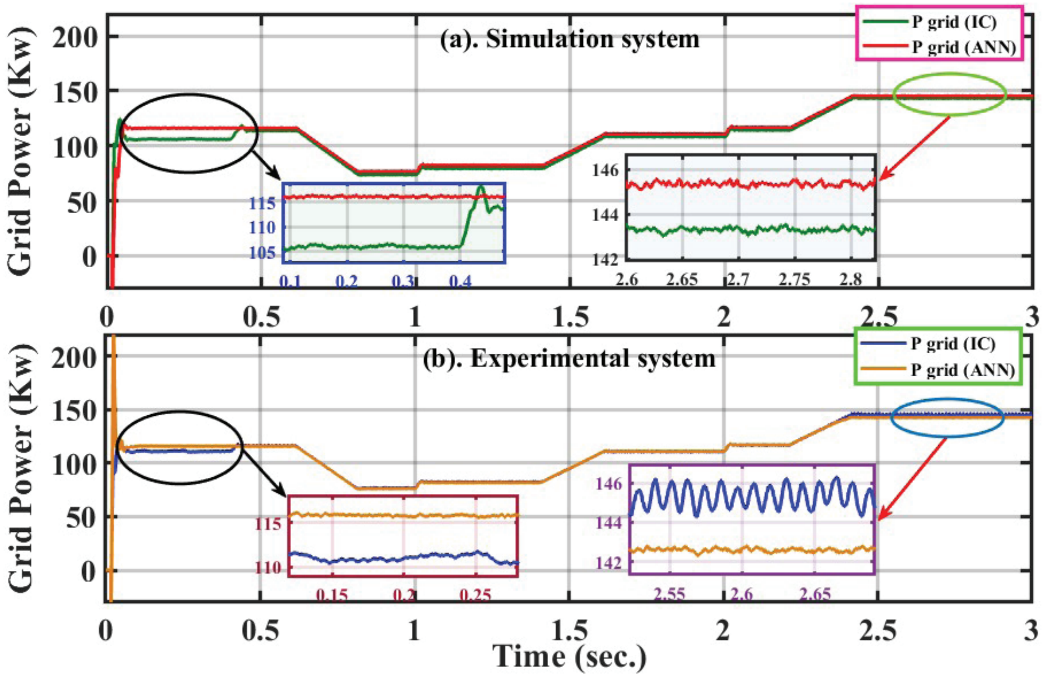

Figure 25: The grid power output system for (a). Simulation system (b). Experimental system.

Table 8: The comparison of MPPT techniques in a hybrid PV/wind power system for simulation and experimental systems

Techniques	Irradiation (W/m²)	Speed of Wind (m/s)	Time (s)	(Kw)		(Kw)		(Kw)		(Kw)	
				Simulink	Experimental	Simulink	Experimental	Simulink	Experimental	Simulink	Experimental
IC	800	7	0.3	70.25	73.88	36.67	36.66	106.92	110.54	105.12	110.48
		7	0.6	78.16	80.43	38.69	38.75	116.85	119.18	113.65	115.03
	400	7	0.9	36.58	39.66	38.68	38.61	75.26	78.27	72.3	76.16
		7.5	1.2	36.54	39.04	43.7	43.56	80.24	82.6	78.25	82.31
ANN	800	7	0.3	80.45	80.06	36.77	36.66	117.22	116.72	116.1	115.83
		7	0.6	80.45	80.04	38.64	38.63	119.09	118.67	116.3	115.78
	400	7	0.9	39.62	39.09	38.72	38.7	78.34	77.79	77.76	77.71
		7.5	1.2	39.62	39.04	43.69	43.7	83.31	82.74	82.85	82.75

A numerical comparison between the simulation and experimental values (see Table 8), where the ANN techniques' actual performance is the best technique, superior efficiency in real-world operation was demonstrated by the ANN technique, which produced the highest P_{Total} and P_{Grid}. The IC technique came in second. Finally, this indicates improved internal consumption control stability and power conversion; its robustness is further supported by its consistent behavior under various wind and radiation conditions. Therefore, the ANN technique stands out as the best choice for practical implementation in hybrid PV/wind systems where maximizing usable energy and ensuring grid efficiency are top priorities. So, the experimental findings reflected the expected behavior based on the simulation analysis, supporting the validity of the model.

VII. Conclusion

This paper presents a hybrid renewable energy grid-connected system for a 150-kW configuration of PV and wind power sources. The dynamic conduct of several MPPT techniques under variable irradiation, temperature, and wind speed profiles is evaluated by MATLAB/Simulink and also is validated by the experimental OPAL-RT platform in real time under Hardware in Loop conditions. According to the obtained results in this paper, there was a great agreement between simulation and experimental results. ANN presented better performance criteria in the comparison with the IC technique in both simulation and experimental validation. The ANN technique reached the minimum error percentage and maximum efficiency in simulation and experimental validation together. Furthermore, the proposed techniques are validated based on the OPAL-RT HIL platform through simulation results. Therefore, these conclusions underline the robustness of the proposed control strategy and its possibility for real-world deployment in large-scale grid-tied-connected PV/wind systems.

References

[1] A. I. Osman *et al.*, “Cost, environmental impact, and resilience of renewable energy under a changing climate: a review,” *Environmental Chemistry Letters*, vol. 21, no. 1, pp. 741–764, Oct. 2022, doi: https://doi.org/10.1007/s10311-022-01532-8.

[2] Y. Xiong and L. Dai, “Does green finance investment impact on sustainable development: Role of technological innovation and renewable energy,” *Renewable Energy*, vol. 214, pp. 342–349, Jun. 2023, doi: https://doi.org/10.1016/j.renene.2023.06.002.

[3] V. Dirma, L. O. Neverauskienė, M. Tvaronavičienė, I. Danilevičienė, and R. Tamošiūnienė, “The Impact of Renewable Energy Development on Economic Growth,” *Energies*, vol. 17, no. 24, pp. 6328–6328, Dec. 2024, doi: https://doi.org/10.3390/en17246328.

[4] Bhanu Ponnapalli, K Lakshmikhandan, Kannan Palanisamy, and Muthukumaran Sithambaram, “A hybrid technique for grid-connected solar–wind hybrid system with electric vehicles,” *Energy & Environment*, vol. 35, no. 5, pp. 2753–2789, Feb. 2023, doi: https://doi.org/10.1177/0958305x231153933.

[5] P. K. Kesavan, U. Subramaniam, D. J. Almakhles, and S. Selvam, “Modelling and Coordinated Control of Grid Connected Photovoltaic, Wind Turbine Driven PMSG, and Energy Storage Device for a Hybrid DC/AC Microgrid,” *Protection and Control of Modern Power Systems*, vol. 9, no. 1, pp. 154–167, Jan. 2024, doi: https://doi.org/10.23919/pcmp.2023.000272.

[6] A. Khan, M. Bressel, A. Davigny, D. Abbes, and B. O. Bouamama, “Comprehensive Review of Hybrid Energy Systems: Challenges, Applications, and Optimization Strategies,” *Energies*, vol. 18, no. 10, pp. 2612–2612, May 2025, doi: https://doi.org/10.3390/en18102612.

[7] T. M. Babu, K. Chenchireddy, K. K. Kumar, V. Nehal, S. Srihitha, and M. R. Vikas, “Intelligent control strategies for grid-connected photovoltaic wind hybrid energy systems using ANFIS,” *International Journal of Advances in Applied Sciences*, vol. 13, no. 3, p. 497, Sep. 2024, doi: https://doi.org/10.11591/ijaas.v13.i3.pp497-506.

[8] N. G. EL Sayed, A. M. Yousef, G. El-Saady, M. D. Alanazi, H. A. Ziedan, and M. Abdelsattar, “Artificial intelligent fuzzy control and LAPO algorithm for enhancement LVRT and power quality of grid connected PV/wind hybrid systems,” *Scientific Reports*, vol. 14, no. 1, Dec. 2024, doi: https://doi.org/10.1038/s41598-024-78384-5.

[9] A. Borni *et al.*, "Enhancing grid connected wind energy conversion systems through fuzzy logic control optimization with PSO and GA techniques," *Scientific Reports*, vol. 15, no. 1, Jul. 2025, doi: https://doi.org/10.1038/s41598-025-12593-4.

[10] A. F. Güven, S. Kamel, and M. H. Hassan, "Optimization of grid-connected photovoltaic/wind/battery/supercapacitor systems using a hybrid artificial gorilla troops optimizer with a quadratic interpolation algorithm," *Neural Computing and Applications*, vol. 37, no. 4, pp. 2497–2535, Dec. 2024, doi: https://doi.org/10.1007/s00521-024-10742-w.

[11] A. F. Tazay, A. M. A. Ibrahim, O. Noureldeen, and I. Hamdan, "Modeling, Control, and Performance Evaluation of Grid-Tied Hybrid PV/Wind Power Generation System: Case Study of Gabel El-Zeit Region, Egypt," *IEEE Access*, vol. 8, pp. 96528–96542, 2020, doi: https://doi.org/10.1109/access.2020.2993919.

[12] S. Najafi-Shad, S. M. Barakati, and A. Yazdani, "An effective hybrid wind-photovoltaic system including battery energy storage with reducing control loops and omitting PV converter," *Journal of Energy Storage*, vol. 27, p. 101088, Feb. 2020, doi: https://doi.org/10.1016/j.est.2019.101088.

[13] P. Gajewski and K. Pieńkowski, "Control of the Hybrid Renewable Energy System with Wind Turbine, Photovoltaic Panels and Battery Energy Storage," *Energies*, vol. 14, no. 6, p. 1595, Jan. 2021, doi: https://doi.org/10.3390/en14061595.

[14] A. Al-Quraan and M. Al-Qaisi, "Modelling, Design and Control of a Standalone Hybrid PV-Wind Micro-Grid System," *Energies*, vol. 14, no. 16, p. 4849, Aug. 2021, doi: https://doi.org/10.3390/en14164849.

[15] A. M. Osman and F. Alsokhiry, "Control design and performance evaluation of a grid connected PV–wind power system: A case study of Dongola, Sudan," *Energy Reports*, vol. 8, pp. 15629–15653, Nov. 2022, doi: https://doi.org/10.1016/j.egyr.2022.11.145.

[16] Y. Kebbati and L. Baghli, "Design, modeling and control of a hybrid grid-connected photovoltaic-wind system for the region of Adrar, Algeria," *International Journal of Environmental Science and Technology*, vol. 20, no. 6, pp. 6531–6558, Aug. 2022, doi: https://doi.org/10.1007/s13762-022-04426-y.

[17] M. Talaat, M. H. Elkholy, A. Alblawi, and T. Said, "Artificial intelligence applications for microgrids integration and management of hybrid renewable energy sources," *Artificial Intelligence Review*, vol. 56, no. 9, pp. 10557–10611, Feb. 2023, doi: https://doi.org/10.1007/s10462-023-10410-w.

[18] Y. Sahri *et al.*, "Performance improvement of Hybrid System based DFIG-Wind/PV/Batteries connected to DC and AC grid by applying Intelligent Control," *Energy Reports*, vol. 9, pp. 2027–2043, Dec. 2023, doi: https://doi.org/10.1016/j.egyr.2023.01.021.

[19] S. Sharma, B. K. Chauhan, and N. K. Saxena, "Artificial Neural Network Grid-Connected MPPT-Based Techniques for Hybrid PV-WIND with Battery Energy Storage System," *Journal of The Institution of Engineers (India) Series B*, vol. 104, no. 6, pp. 1217–1226, Oct. 2023, doi: https://doi.org/10.1007/s40031-023-00922-y.

[20] A. M. Alatwi, A. Bakeer, S. A. Zaid, I. E. Atawi, H. Albalawi, and A. M. Kassem, "Intelligent Fractional-Order Controller for SMES Systems in Renewable Energy-Based Microgrid," *Computer Modeling in Engineering & Sciences*, vol. 140, no. 2, pp. 1807–1830, 2024, doi: https://doi.org/10.32604/cmes.2024.048521.

[21] A. Rashid and A. Zubair, "Artificial Neural Network MPPT and Intelligent Energy Management for Grid-Integrated Hybrid PV-Wind-Battery Systems," *2025 International Conference on Green Energy, Computing and Sustainable Technology (GECOST)*, pp. 1–6, Nov. 2025, doi: https://doi.org/10.1109/gecost66002.2025.11325022.

[22] M. E.-S. M. Essa, A. S. S. Ahmed, E. E. El-Kholy, and H. E.-S. Awad, "MPPT based- ANN for PV Solar-Powered Electric vehicle charging Stations," in *2025 26th International Middle East Power Systems Conference (MEPCON)*, 2025, pp. 1–7.

[23] Z. Reguieg, F. Mehedi, I. Bouyakoub, W. M. Kacemi, F. Saidi, and S. Mekhilef, "ANN-based PV-integrated power conditioning system for MPPT optimization and power quality enhancement in hybrid microgrids," *Energy Reports*, vol. 15, p. 109129, Jun. 2026, doi: https://doi.org/10.1016/j.egyr.2026.109129.

[24] H. mohammadi, M. Radmehr, T. Nouri, and A. Ghafouri, "Optimization of maximum power point tracking in a wind-solar hybrid power plant by neural networks for reducing total harmonic distortion (THD)," *Energy Informatics*, vol. 9, no. 1, Jan. 2026, doi: https://doi.org/10.1186/s42162-026-00620-1.

[25] A. M. Hemeida, M. El-Ahmar, A.-H. Ahmed, and H. M. Hasanien, "Optimum design of hybrid wind/PV energy system for remote area," *Ain Shams Engineering Journal*, vol. 11, no. 1, pp. 11–23, Mar. 2020, doi: https://doi.org/10.1016/j.asej.2019.08.005.

[26] O. Bautista, Á. Bernal, A. Pantoja, and J. Revelo, "FPGA Implementation of a PV Generator and a Boost Converter Controllers for a Virtual Laboratory Environment," *Iranian Journal of Science and Technology Transactions of Electrical Engineering*, vol. 48, no. 2, pp. 533–551, Mar. 2024, doi: https://doi.org/10.1007/s40998-024-00704-2.

[27] Ch. P. Kumar, S. Pragaspathy, V. Karthikeyan, and S. Durga, "Power Quality Improvement for a Hybrid Renewable Farm Using UPQC," in *2021 International Conference on Artificial Intelligence and Smart Systems (ICAIS)*, Mar. 2021. doi: https://doi.org/10.1109/icais50930.2021.9396048.

[28] G. Mayilsamy *et al.*, "A Review of State Estimation Techniques for Grid-Connected PMSG-Based Wind Turbine Systems," *Energies*, vol. 16, no. 2, pp. 634–634, Jan. 2023, doi: https://doi.org/10.3390/en16020634.

[29] A. Khan, D. A. Aragon, M. Seyedmahmoudian, S. Mekhilef, and A. Stojcevski, "Inertia emulation control of PMSG-based wind turbines for enhanced grid stability in low inertia power systems," *International Journal of Electrical Power & Energy Systems*, vol. 156, pp. 109740–109740, Jan. 2024, doi: https://doi.org/10.1016/j.ijepes.2023.109740.

[30] A. Q. Al-Shetwi, M. A. Hannan, K. P. Jern, A. A. Alkahtani, and A. E. PG Abas, "Power Quality Assessment of Grid-Connected PV System in Compliance with the Recent Integration Requirements," *Electronics*, vol. 9, no. 2, p. 366, Feb. 2020, doi: https://doi.org/10.3390/electronics9020366.

[31] Z. Dong and C. Liu, "Three-Dimension Space Vector Modulation for Three-Phase Series-End Winding Voltage-Source Inverters," *IEEE Transactions on Industrial Electronics*, vol. 71, no. 1, pp. 82–92, Jan. 2024, doi: https://doi.org/10.1109/tie.2023.3241399.

[32] C. S. Yee, S. A. Azmi, L. J. Hwai, M. F. N. Tajuddin, M. Z. A. Zahari, and S. R. A. Rahim, "Comparative Evaluation of Three-Phase Inverter Topologies Based on Voltage Boosting Features," *Journal of Physics: Conference Series*, vol. 2641, no. 1, p. 012021, Nov. 2023, doi: https://doi.org/10.1088/1742-6596/2641/1/012021.

[33] D. Salman, Y. K. Elmi, A. M. Isak, and A. Sheikh-Muse, "Evaluation of MPPT Algorithms for Solar PV Systems with Machine Learning and Metaheuristic Techniques," *Mathematical Modelling of Engineering Problems*, vol. 12, no. 1, pp. 115–124, Jan. 2025, doi: https://doi.org/10.18280/mmep.120113.

[34] H. A. Kazem *et al.*, "Performance evaluation of solar photovoltaic/thermal system performance: An experimental and artificial neural network approach," *Case Studies in Thermal Engineering*, vol. 61, p. 104860, Jul. 2024, doi: https://doi.org/10.1016/j.csite.2024.104860.

[35] M. A. B. Siddique, A. Asad, R. M. Asif, A. U. Rehman, M. T. Sadiq, and I. Ullah, "Implementation of Incremental Conductance MPPT Algorithm with Integral Regulator by Using Boost Converter in Grid-Connected PV Array," *IETE Journal of Research*, vol. 69, no. 6, pp. 1–14, May 2021, doi: https://doi.org/10.1080/03772063.2021.1920481.

[36] A. F. Abouzeid, H. Eleraky, A. Kalas, R. Rizk, M. M. Elsakka, and A. Refaat, "Experimental validation of a low-cost maximum power point tracking technique based on artificial neural network for photovoltaic systems," *Scientific Reports*, vol. 14, no. 1, Aug. 2024, doi: https://doi.org/10.1038/s41598-024-67306-0.

[37] M. Jlidi, O. Barambones, F. Hamidi, and M. Aoun, "ANN for Temperature and Irradiation Prediction and Maximum Power Point Tracking Using MRP-SMC," *Energies*, vol. 17, no. 12, p. 2802, Jun. 2024, doi: https://doi.org/10.3390/en17122802.

[38] R. R. Elbanna, M. H. ElMessmary, H. Diab, and M. Abdelsalam, "A smart hybrid optimization model for DSSE in renewable energy-powered distribution networks," *Renewable Energy and Sustainable Development*, vol. 11, no. 2, p. 314, Sep. 2025, doi: https://doi.org/10.21622/resd.2025.11.2.1271.

[39] S. Kumar, I. Ali, and A. S. Siddiqui, "Real time operation of microgrid with variation of distribution generation source to IEEE 13 bus system," *Renewable Energy and Sustainable Development*, vol. 11, no. 2, p. 424, Nov. 2025, doi: https://doi.org/10.21622/resd.2025.11.2.1572.

[40] R. S. Hiware and P. M. Daigavane, "Super capacitor-enhanced neural control (SENCO) for power quality optimization in wind turbine-integrated microgrids," *Renewable Energy and Sustainable Development*, vol. 11, no. 2, p. 273, Aug. 2025, doi: https://doi.org/10.21622/resd.2025.11.2.1279.

[41] O. M. Abo Gabl, M. Y. Morgan, and M. S. El-Sobki (Jr.), "Decentralized economic operation of isolated AC, DC, and hybrid microgrids," *Renewable Energy and Sustainable Development*, vol. 11, no. 2, p. 175, Aug. 2025, doi: https://doi.org/10.21622/resd.2025.11.2.1289.

[42] A. M. Noman, H. Khan, H. A. Sher, S. Z. Almutairi, M. H. Alqahtani, and A. S. Aljumah, "Scaled Conjugate Gradient Artificial Neural Network-Based Ripple Current Correlation MPPT Algorithms for PV System," *International Journal of Photoenergy*, vol. 2023, no. 1, pp. 1–8, Jun. 2023, doi: https://doi.org/10.1155/2023/8891052.

[43] Y. Ledmaoui *et al.*, "Enhancing Solar Power Efficiency: Smart Metering and ANN-Based Production Forecasting," *Computers*, vol. 13, no. 9, pp. 235–235, Sep. 2024, doi: https://doi.org/10.3390/computers13090235.

[44] M. T. Hussain, A. Sarwar, M. Tariq, S. Urooj, A. BaQais, and M. A. Hossain, "An Evaluation of ANN Algorithm Performance for MPPT Energy Harvesting in Solar PV Systems," *Sustainability*, vol. 15, no. 14, p. 11144, Jan. 2023, doi: https://doi.org/10.3390/su151411144.

[45] N. Ncir and N. El Akchioui, "An Intelligent Improvement Based on a Novel Configuration of Artificial Neural Network Model to Track the Maximum Power Point of a Photovoltaic Panel," *Journal of Control, Automation and Electrical Systems*, vol. 34, no. 2, pp. 363–375, Nov. 2022, doi: https://doi.org/10.1007/s40313-022-00972-5.

[46] M. Yilmaz, R. Celikel, and A. Gundogdu, "Enhanced Photovoltaic Systems Performance: Anti-Windup PI Controller in ANN-Based ARV MPPT Method," *IEEE Access*, vol. 11, pp. 90498–90509, Jan. 2023, doi: https://doi.org/10.1109/access.2023.3290316.

[47] A. Ahmad and R. Loganathan, "Real-Time Implementation of Solar Inverter with Novel MPPT Control Algorithm for Residential Applications," *Energy and Power Engineering*, vol. 5, no. 6, pp. 427–435, 2013, doi: https://doi.org/10.4236/epe.2013.56046.

[48] B. Mohapatra *et al.*, "Optimizing grid-connected PV systems with novel super-twisting sliding mode controllers for real-time power management," *Scientific Reports*, vol. 14, no. 1, p. 4646, Feb. 2024, doi: https://doi.org/10.1038/s41598-024-55380-3.

[49] M. Mohamed, Z. M. Alaas, B. A. Faiya, H. Y. Hegazy, W. I. Mohamed, and S. A. M. Abdelwahab, "Performance Improvement of Grid-Connected PV-Wind Hybrid Systems Using Adaptive Neuro-Fuzzy Inference System and Fuzzy FOPID Advanced Control With OPAL-RT," *IEEE Access*, vol. 13, pp. 55996–56020, 2025, doi: https://doi.org/10.1109/access.2025.3548926.